Crashworthiness of the Flying-V Aircraft Concept with Vertical Drop Test Simulations

Marco Desiderio, Michiel J. Schuurman, René Alderliesten and Saullo G.P. Castro[*].

Department of Aerospace Structures and Materials, Faculty of Aerospace Engineering, Delft University of Technology, Kluyverweg Street No. 1, 2629HS, Delft, The Netherlands.

The following presents a preliminary assessment on the crash characteristics of the Flying-V aircraft, an unconventional configuration consisting of a V-shaped flying wing with an oval cabin cross section, currently being actively researched at TU Delft. Successively, the preliminary assessment is carried out by means of design of experiments, where four crash structure concepts are defined and evaluated. Virtual drop tests of the Flying-V typical fuselage section are performed while measuring the energy absorption of the fuselage, and the dynamic response index (DRI) and selected locations. The finite element modeling scheme is validated using the Fokker F-28 Fellowship typical section, for which physical drop test data is available. While a crashworthy typical section for the Flying-V could not be designed, it has been found that a conventional crash concept with a total of four oblique floor struts is able to absorb 72% of the total kinetic energy, with a DRI reaching 18.2 units. A sensitivity analysis shows that the bending stiffness of the frames has a critical role in the crashworthiness of the Flying-V, due to the increase in rigidity following pressurization loads of the oval fuselage section and that, additionally, the structural simplifications applied in the context of the research likely rendered the results overly-conservative. A 16% frame thickness reduction resulted in a DRI of 16.2 units, just above the 16 units typically required by regulators. Recommendations for future work include a structural sizing optimization where requirements from crashworthiness and airworthiness can be evaluated simultaneously as design constraints, enabling design for crashworthiness at the preliminary design.

I. Introduction

The Flying-V aircraft[1] (FV) is a novel aircraft configuration being researched at the Delft University of Technology (TU Delft). In the FV, the cabin and two-half-wings have been integrated to form a V-shaped aircraft [1], in a configuration that promises higher aerodynamic efficiency and an estimated 20% reduction in fuel burn [2]. Compared to other blended wing-body designs, the Flying-V can be stretched to generate a family of designs, thus rendering this concept more palatable from a commercial standpoint [2]. Contrarily to conventional aircraft configurations, the Flying-V cabin's typical section presents a significant eccentricity that creates unprecedented challenges for the cabin crashworthiness.

Part of the research performed at TU Delft on the FV focuses on safety, with bird strike being an aspect critically affecting the crashworthiness of the Flying-V, as investigated by Chen et al. [3]. The current research aims to provide a preliminary assessment on the crashworthiness characteristics of the Flying-V fuselage undergoing a vertical drop test. The approach herein proposed starts with the definition of four different crash concepts which are successively evaluated by means of virtual drop test based on explicit dynamic finite element analysis, using a model including five frames along the typical fuselage cross section. A total of 74 simulations are run, each involving different thicknesses and positioning of the crushable elements. All the different concept variants have subsequently been compared in terms of the dynamic response index (DRI), energy absorption characteristics, and mass of the crushable structure.

II. Concepts Definition

As a reference, the general layout of the Flying-V is shown in Fig. 1a[1]. The structural layout of the typical wing-fuselage section consists of a main trailing edge spar, stiffened skin and frames, and a cross beam, as illustrated in Fig. 1b. A high-level sizing of the airframe components was performed by Dotman [4], where for each member

---

(a) The Flying-V aircraft. The red box indicates the FV's fuselage section being investigated.

(b) Structural layout of the typical fuselage section of the FV. Adapted from [4].
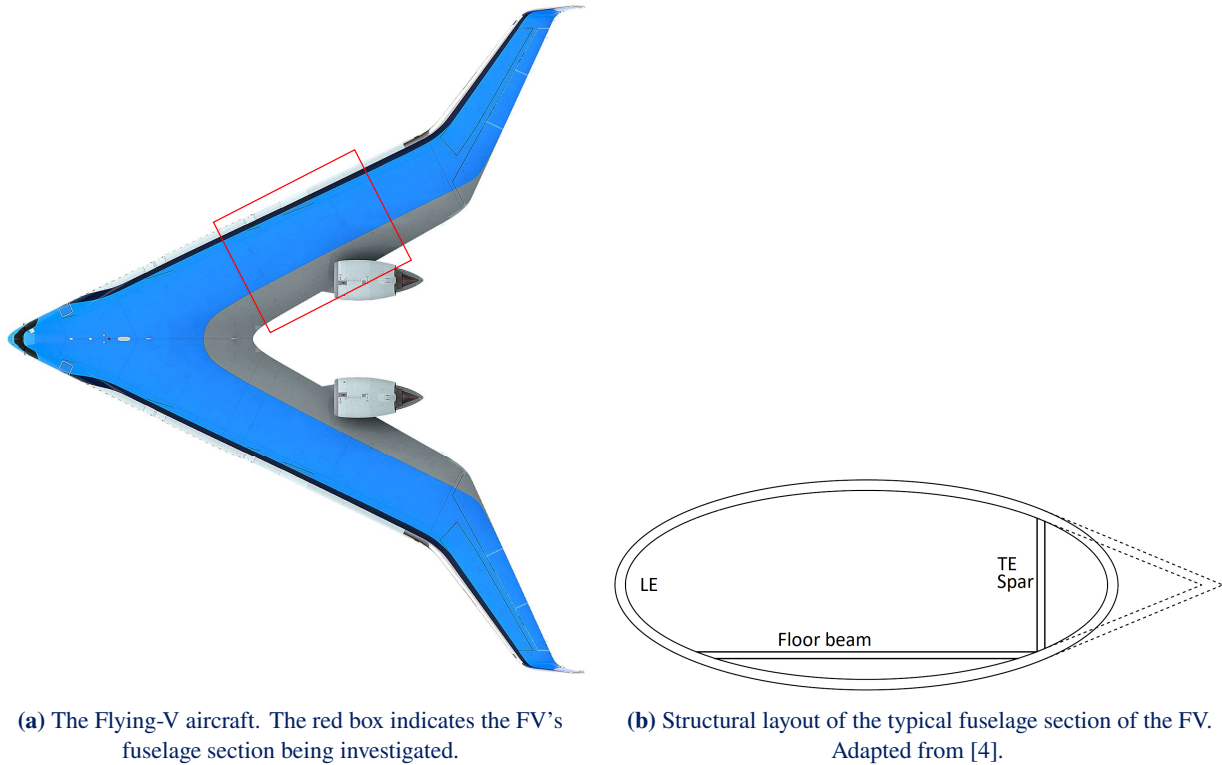
Fig. 1: Flying-V aircraft concept (a) and typical fuselage section structural layout (b).

a cross-section shape has first been defined and, successively, the thickness and beam cross-section height were optimized. The driving load case for the sizing of the frames was the fuselage pressurization, due to the oval shape of the wing-fuselage that tends to become circular under pressurization. Hence, the frames need to be sufficiently stiff and strong such that the oval shape is preserved.

In the context of the present research, the constraints relative to the floor vertical location and beam sizing are relaxed, making them design variables. The impact of this relaxation on the overall airframe stiffness and strength is however unknown. However, an increase in the stiffness of the is hypothesized to be required: Dotman has observed that pressurization induces a compressive load in the cross beams because the oval shape tends to open; thus, an increase in the height or thickness of the frames would be required to compensate for the loss of the cross beams' stiffness. This last statement is written with the after-thought that, as it will be shown later, a more flexible cross beam is beneficial for crashworthiness.

Of the four concepts defined, two consist of a conventional floor struts configuration and include a total of four and six struts, hereinafter defined as '4S' and '6S', respectively, as shown in Fig. 2a and Fig. 2b.

In concepts 4S and 6S the considered design variables are the positioning and thickness of the floor struts, and thickness of the cross beam. The other two concepts herein referred to as HB and HBH, employ horizontal beams and vertical struts to support the cross beams and dissipate energy during a crash. Their difference is that in HB only one horizontal beam is present, whereas in HBH a set of horizontal beams and vertical struts are arranged in a hierarchical pattern. Both HB and HBH are illustrated in Fig. 3 and Fig. 4. The design variables considered for these concepts are the wall thickness, and horizontal and vertical positioning of the beams and struts.

III. Finite Element Representation

The final element model (FEM) consists of a five-frame section of the FV aircraft. For general certification purposes, a six-frame typical section is used since, on average, it has the same stiffness and mass properties of a larger fuselage [5]. This hypothesis is tested and data from Appendix A shows that, in fact, little difference is observed in the crash behavior between a five- and a six-frame section. In order to reduce the computational cost of the explicit analyses, it is decided
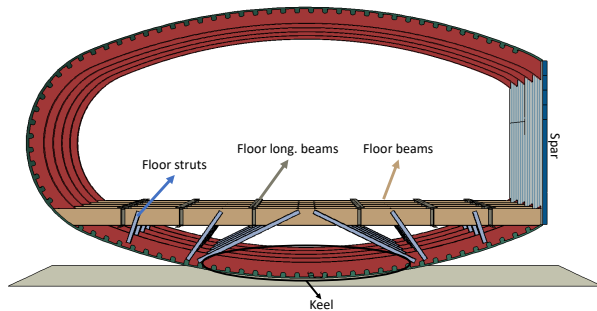
(a) Fuselage section depicting the 6S concept, including components nomenclature. Skin and frames have been left unlabeled for the sake of clarity.
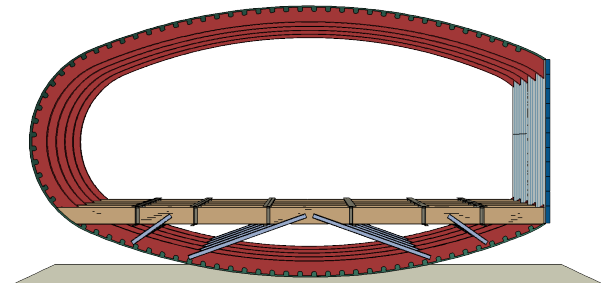
(b) Fuselage section depicting the 4S concept.

Fig. 2: Fuselage sections depicting 6S (a) and 4S (b) floor struts concepts. Across different concepts of the same family, the floor strut positioning (rotation and translation) is a design variable. Different colors are qualitatively indicative of different section assignments.
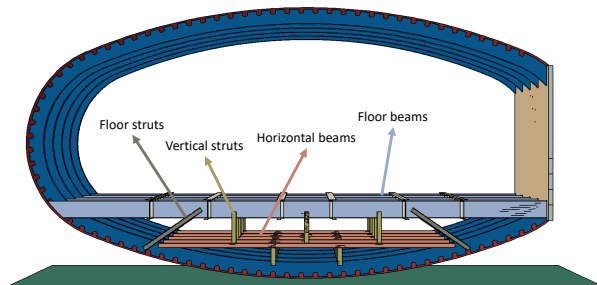

Fig. 3: Fuselage section depicting the HB crash concept configuration, including components nomenclature. Vertical struts thickness and positioning, as well as the horizontal beam thickness and cross-section have been varied across variations of this concept.
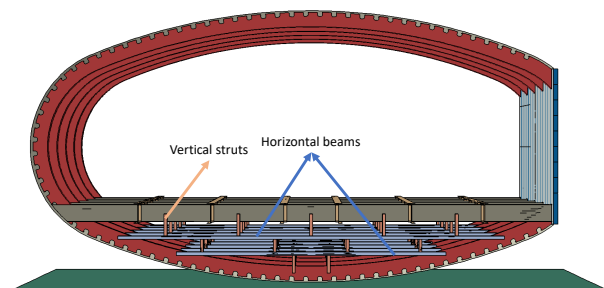
Fig. 4: HBH concept configuration. The thickness and positioning of the vertical struts, as well we the cross-section and thickness of the horizontal beams have been treated as geometric variables.

to thus include five frames only.

The FEM is built using exclusively shell elements, considering that all the structural features of the fuselage section are made out of plates, whose thickness is significantly smaller than the other two dimensions. The mesh is quad-dominated using fully integrated first-order elements (S4), which are well-suited for impact dynamics problems [6]. The assigned global element size and thicknesses for each structural component are shown in Tab. 1.

Tab. 1: General element sizes for different structural components. The notation 'var' indicates that the thickness assignment is a design variable.

Item	Elem. size [mm]	Thick. [mm]	Item	Elem. size [mm]	Thick. [mm]
Skin	60	2	Ground	200	3
Frames	20	5.7	Floor beams	30	var
Floor long. beams	20	2	Floor struts	10	var
Spar skin	20	3	Horiz. beams	10	var
Spar stiffeners	20	3	Vert. struts	10	var

In terms of material, the current design of the FV aircraft makes wide use of the 2024-T3 aluminium alloy [4]. The properties for this alloy, taken from literature, are presented in Tab. 2.

The chosen material model to be used in the simulation is the Johnson-Cook model (JC), an elastic-plastic model which can also include temperature and strain-rate dependencies. It is computationally efficient and widely used in industry for impact damage simulations [7]. In the JC model, the flow stress is defined by the following relation [7]:

$$\sigma_y = \left(A + B\bar{\varepsilon}^{p^n}\right)(1 + c \ln \dot{\varepsilon}^*)(1 - T^{*m}) \tag{1}$$

with A and B being the material yield strength and hardening modulus respectively, $\bar{\varepsilon}^p$ the plastic strain, n hardening parameter, $\dot{\varepsilon}^*$ the strain rate, c the strain-rate dependency parameter, T^* the dimensionless temperature ($T^* = \frac{T - T_{\text{room}}}{T_{\text{melt}} - T_{\text{room}}}$) and, lastly, m the temperature dependency parameter.

The employed failure model is a strain-based one [7]:

$$\varepsilon_{\text{failure}} = [D_1 + D_2 \exp(D_3\sigma^*)][1 + D_4 \ln(\varepsilon^*)][1 + D_5 T^*] \tag{2}$$

with D_1 to D_5 being empirically-determined failure parameters. σ^* is the pressure-to-effective stress ratio:

$$\sigma^* = \frac{\text{pressure}}{\bar{\sigma}} \tag{3}$$

In the JC model, fracture occurs when the damage parameter $D > 1$, being D the ratio between the effective plastic strain and the failure strain, determined using (2):

$$D = \sum \frac{\Delta\bar{\varepsilon}^p}{\varepsilon_{\text{failure}}} \tag{4}$$

Tab. 2: Parameters used for JC elastic-plastic model, including damage [7]. c, n, m, D_4 and D_5 have been set to zero considering the strain-rate insensitivity of AA2024-T3, and that all analyses are performed at room temperature. All units in kg, N and mm.

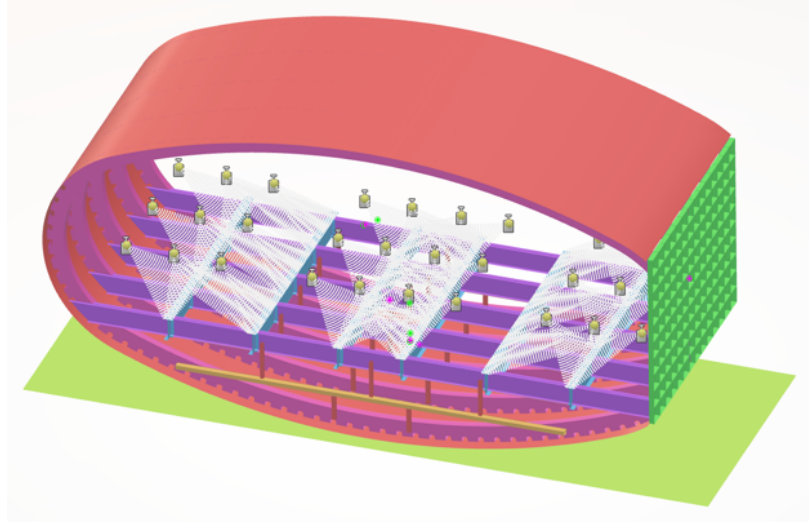| Variable	Value	Variable	Value
A	369	D_1	0.112
B	684	D_2	0.123
c	0	D_3	1.5
n	0.73	D_4	0
m	0	D_5	0

Fig. 5: View of the FEM of the FV aircraft; HB-5 concept.

Lastly, all riveted connections are modeled by means of tie constraints in order to avoid failure at the joint: by design, failure of joins is undesired and, therefore, as shown experimentally [8, 9], in a crash scenario this is unlikely to happen. It is therefore decided to completely remove the possibility of this occurring in the current model.

In order to avoid element penetration, a general contact interaction property is defined, where the normal behavior is a hard contact, whereas the tangential behavior is defined using a penalty friction formulation, by specifying the friction coefficient. The chosen friction coefficient is 0.5 (slip-rate independent)[2], which is a reasonable estimate for both aluminum/aluminum and aluminum/asphalt contact interfaces.

The assumed mass of a single passenger is of the 95th percentile male, equal to approximately 90 kg [10]. Additionally, further 10 kg have been allocated to account for the seat mass[3]. The total mass of the passenger and seat system is thus of 100 kg, and, in the FEA, has been modeled as a point inertia.

The seat is modeled by means of a flexible coupling with the floor structure. Reference values in the literature on the stiffness of airliner seats were not readily available; the opposite is true for general aviation (GA) ones. According to Alfaro-Bou et al. [11], GA aircraft typical seats have a stiffness of approximately 365 N/mm. GA aviation seats are expected to be more compliant than commercial aviation (CA) ones, considering the larger vertical speeds and thus accelerations that occur during the landing phase of CA aircraft. Consequently, the chosen spring constant in the FEM used to model the seat has been of 3924 N/mm, which is approximately a factor of 11 stiffer than GA sheet-metal seats.

The fuel mass is not included in the analysis, as typically done for drop test simulations. In its current configuration, the fuel is stored aft of the Flying-V wing-fuselage spar. As reference, a visual representation of the FEM if given in Fig. 5. Model validation was performed by first performing a similar crash analysis using the typical section of an aircraft for which drop test data is readily available, and successively expand the model to the FV. The typical section drop test used for validation is that of a Fokker F-28 Fellowship, performed by NASA in the early 2000s [8]. Information regarding model validation can be found in Appendix A.

IV. Concepts Evaluation

The proposed concepts are evaluated in terms of dynamic response index (DRI) and energy absorption characteristics.

A. Criteria and Requirements

The DRI is a method used since the 1970s by the US Air Force (USAF) to determine the probability of spinal injuries in pilots subjected to the high-amplitude and short-duration accelerations induced by ejection seats [12]. With the DRI, the total body mass acting upon the vertebrae is modeled as a point mass, thereby yielding the following

---

[2]`https://www.engineeringtoolbox.com/friction-coefficients-d_778.html`. Accessed on 24-May-2023.
[3]`https://www.recaro-as.com/en/aircraft-seats/economy-class/sl3510.html`. Accessed on 24-May-2023.
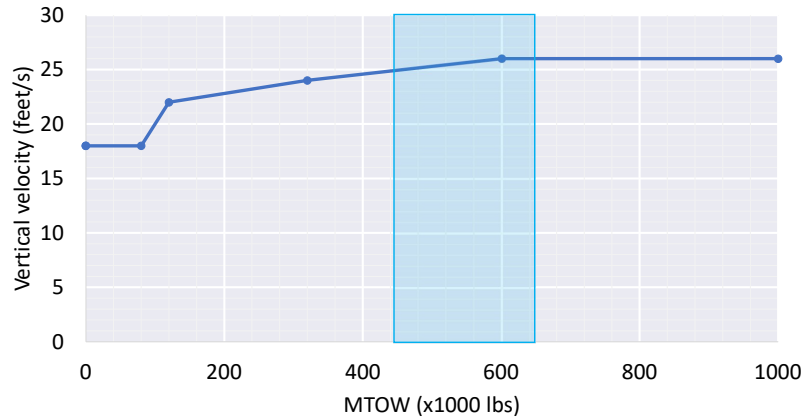
Fig. 6: Vertical impact velocity requirement vs. MTOW, adapted from TACDWG [15]. The blue region indicates the estimated range of MTOW for the Flying-V family, as determined by Oosterom [2].

differential equation [13]:

$$\frac{d^2\delta}{dt^2} + 2\zeta\omega_n\frac{d\delta}{dt} + \omega_n^2\delta = z \tag{5}$$

which is a typical equation for a single degree of freedom (SDOF) spring-dashpot model with external acceleration input; where δ represents the degree of freedom, ζ the damping ratio, $\omega_n = \sqrt{\frac{k}{m}}$ the natural frequency with k being the spring stiffness constant and m the point mass, and z the acceleration input. For instance, Stech and Pain [14] found ω_n =52.9 rad/s and ζ =0.224 for the 50th percentile of USAF pilots at the time. The DRI is generally correlated with a probability of spinal injury; however, since this method has been in use at USAF since the 1970s, the actual accuracy of such probability function is disputable, as it was derived decades ago based on injury data from a sample (USAF) that lacked diversification in terms of age, gender, and body type. It is nevertheless a good baseline for comparison [15]. At the time of the writing of this article, no explicit requirements exist in CS-25 or 14 CFR Part 25 regarding spinal injury following a crash landing [16, 17]. However, in 2018, the Transport Aircraft Crashworthiness and Ditching Working Group (TACDWG), a commission instituted by the Federal Aviation Administration's Aviation Rulemaking Advisory Committee (ARAC) with the purpose of providing recommendations for new airframe-level crashworthiness and ditching standards, recognized that:

- DRI of 16 units is an acceptable limit for crashworthiness certification, as it has been deemed already so by regulatory agencies in previously certified aircraft;
- The vertical impact velocity requirement is to be determined according to the aircraft's maximum take-off weight (MTOW), as illustrated in the envelope of Fig. 6.

Since the focus of this assessment will be the FV's typical section, it will need to be designed according to the most stringent requirement. The MTOW of the heaviest FV variant is estimated to be $278 \cdot 10^3$ kg ($613 \cdot 10^3$ lbs) [2], corresponding to a vertical impact speed of 26 feet/s. In the context of this research the DRI will be determined for each point-inertia. For concept comparison, a single 'equivalent' DRI number is then determined, defined be a weighted average of DRIs for different seats, such that the likelihood of spinal injury is the same as if a DRI of 16 units was measured at each seat location.

Other than the DRI, the energy-absorption characteristics of the different concepts are also evaluated in terms of the overall amount of energy dissipated, and a breakdown by component; as well as the crushable structure's mass fraction compared to the total section weight.

B. Evaluation

The total mass of the sections ranges between 3878 kg (4S-2) to 3907 kg (HB-3) and is distributed in the following manner:

- 3000 kg for passenger and seats mass;
- 83 kg for the (aft) spar mass; the accuracy of such value is unknown due to the lack of sizing data in this regard;

- 262 kg for the skin. This value overestimates the actual skin mass, as the assumed skin thickness is the largest one computed by Dotman [4];
- 443 kg for the frames;
- 44 kg for the floor longitudinal beams (seat rails);
- The crushable mass (variable), defined as the mass of all components treated as design variable: cross beams the supporting structure.

A high-level comparison of all concepts is given in Tab. 3, where the averaged DRI, the fraction of initial kinetic energy dissipated, specific energy absorption (SEA) and the crushable mass fractions are shown for all concept configurations. The SEA is determined by dividing the total energy absorbed by the crushable mass. For all concepts, the mass fraction of the crushable structure ranges between 1.2% and 2%, when compared to the total mass of the analyzed section. This means that the pre-crash kinetic energy for all sections is comparable, and that the crushable mass will have little influence on the overall mass of the section.

In Tab. 3, different configurations of the same concept are denoted with a $-n$, indicating that the position of the crash structure elements has been changed. For the same configuration, multiple analyses were run for different thicknesses of crash structure components; and these are defined as variants of the same configuration hereinafter. The first observation to be made is that, none of the analyzed sections are able to meet the 16 DRI units requirement, with the lowest one being of 18.2. As investigated later in section V, this is mainly caused by an overly-conservative approximation of the fuselage frames: in Dotman's study, the fuselage frames were optimized and have variable height and thickness. Within the present research, for the sake of modeling simplicity, the frame thickness is taken as constant and the largest value is used, while the height is averaged. These simplifications could have caused a conservative estimate of the frames' bending stiffness, resulting in a harder impact.

From the acquired simulation data, concept 6S is able to absorb approximately the same energy fraction of 4S-1 and 4S-5, whereas the equivalent DRI being significantly higher due to 6S being significantly stiffer than 4S. This extra stiffness comes from the two extra struts in the vicinity of the attachment between the floor cross beams and the frames, which is a region that is already stiff on its own. The presence of the additional struts limits compliance, causing an increase in the observed accelerations. Thus, concept 6S was discarded at the very beginning of the study, meaning that no further iterations have been performed on it.

Tab. 3: DRI, fraction of initial kinetic energy dissipated, SEA and crushable mass as a fraction of the total section mass, for the best configuration of each concept.

Version	DRI [-]	$\frac{E_D}{K_{EG}}$ [%]	SEA [kJ/kg]	$\frac{m_{crush}}{m_{tot}}$ [%]	Version	DRI [-]	$\frac{E_D}{K_{EG}}$ [%]	SEA [kJ/kg]	$\frac{m_{crush}}{m_{tot}}$ [%]
6S-1	23.5	72	1.35	1.64	HB-2	23.9	71	1.07	2.05
4S-1	23.1	73	1.84	1.24	HB-3	24.5	70	1.11	1.97
4S-2	20.4	78	1.99	1.22	HB-4	23.4	70	1.26	1.74
4S-3	20.0	77	1.74	1.37	HB-5	24.6	64	1.15	1.75
4S-4	18.9	76	1.51	1.60	HBH-1	24.9	66	1.19	1.74
4S-5	18.2	72	1.47	1.60	HBH-2	24.4	68	1.19	1.78
HB-1	22.2	69	1.27	1.76	HBH-3	24.8	67	1.19	1.75

Fig. 7 further shows the equivalent DRI determined for each analyzed section, which is plot with the dissipated energy normalized by the pre-impact kinetic energy. In general, a downward trend is observed showing that for the same configuration or concept, variants that dissipate a larger amount of kinetic energy are also able to better protect the occupants with lower DRI values. Clearly, concept 6S is shown to have the highest DRI of all. The design envelope for concept 4S, in turn, is wider than for all other concepts, indicating that a large variety of designs can be achieved. HB and HBH occupy approximately the same space in the DRI-normalized energy envelope, as they feature many similarities. As discussed later in this article, the crushable structure of concepts HB and HBH are subjected to structural instability and are not able to be crushed as intended, therefore not absorbing as much energy as intended. The structural instability observed in HB and HBH also explains the relatively smaller design envelope for those two concepts, when compared to 4S or 6S.

In terms of SEA, a similar graph is shown in Fig. 8, where the specific energy absorption is present on the horizontal axis instead of the normalized energy. Once again, concept 4S has the largest design envelope of all, whereas HB and
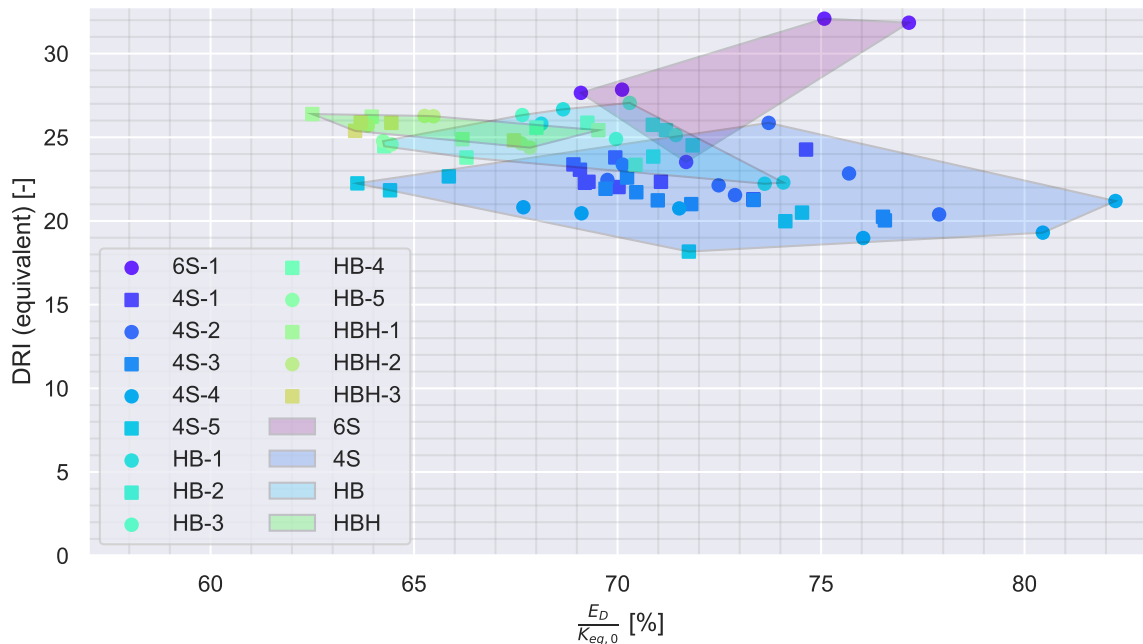
Fig. 7: Equivalent DRI versus the dissipated energy normalized by the pre-impact kinetic energy, for all the tested variants. In general, concept configurations that are able to dissipate more energy result in lower DRI levels. This is not the case for concept 6S, due to the high stiffness provided by the two additional struts when compared to concept 4S.

HBH have similar SEA due to the aforementioned observed structural instability.

1. 4S Concept

As shown in Tab. 3, the best performing configuration for the 4S concept in terms of DRI is the 4S-5, which is the concept with the lowest DRI across all the analyzed cross sections. The pre- and post-crash sections of all the five different $4S-n$ configurations are presented in Fig. B.1 and Fig. B.2. While, locally, some plastic deformation occurs at the location where the floor struts are joined to the fuselage frames, the frames as a whole still do remain largely undeformed, forcing more energy to be absorbed by the floor cross beams and struts, as shown in Fig. 9. For variants with larger floor struts thicknesses, the buckling and crippling loads are increased leading to higher failure loads that enable more plasticity at the frames. This shows that, overall, thicker floor struts alone do not dissipate more energy, but they can however induce more plastic deformation elsewhere.

Another reason to why thicker floor struts alone do not dissipate more energy comes from the fact that, once the floor struts buckle, they start to fold such that the energy-absorbing capabilities of this deformation mechanism are not significantly affected by an increase in thickness, and more dependent on the geometry of the strut cross section. This is particularly evident when comparing variants with 1 mm floor cross beam thickness, and 2 mm and 2.5 mm floor struts thicknesses; where the energy absorption of the frames increases significantly, while that of the cross beam and of the struts actually decreases. In essence, the floor struts are able to transfer the load from the floor cross beams to the frames, resulting in less deformation and therefore less energy absorbed by the struts themselves; and while preventing the cross beam from deforming significantly.

Lastly, regarding the energy dissipated by plastic deformation of the skin, the simulation data shows that, for configurations with thicker floor struts the skin also dissipates more energy. This phenomenon is correlated with the plastic deformation of the frames to which the skin is tied. When the frames bend, the skin deforms with them, and, as mentioned, thicker floor struts favor the bending of the frames.
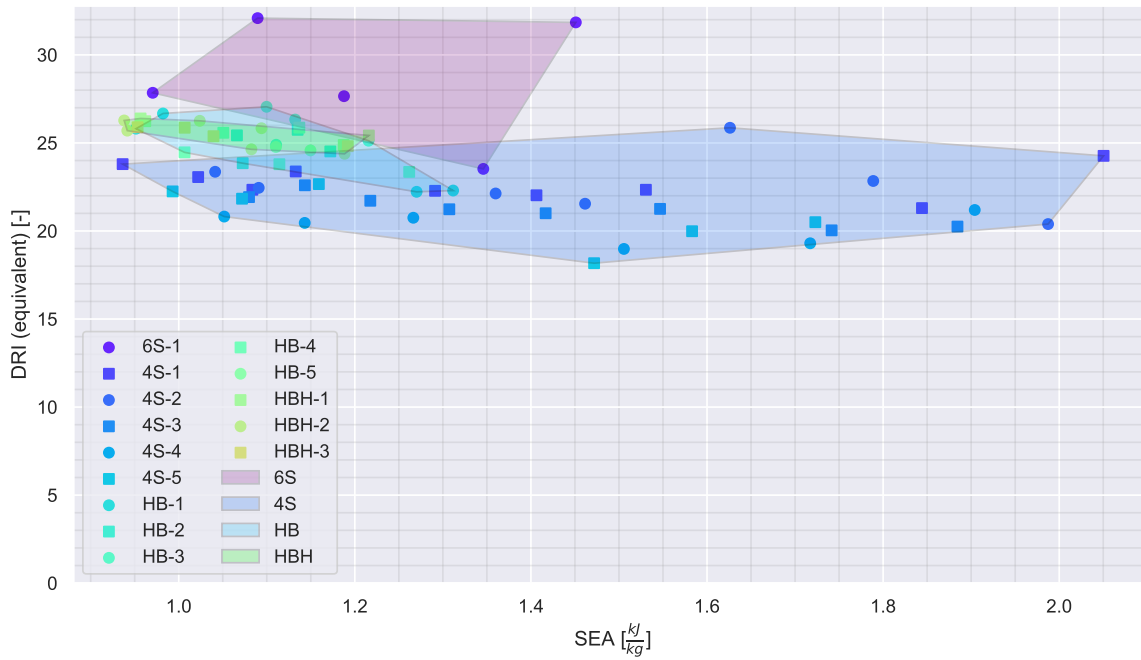
Fig. 8: DRI versus the specific energy absorption of floor cross beams and crash structure (SEA). For concepts HB and HBH, it can be observed that configurations with higher SEA will also have a lower DRI, since the crushable structure is more effective.
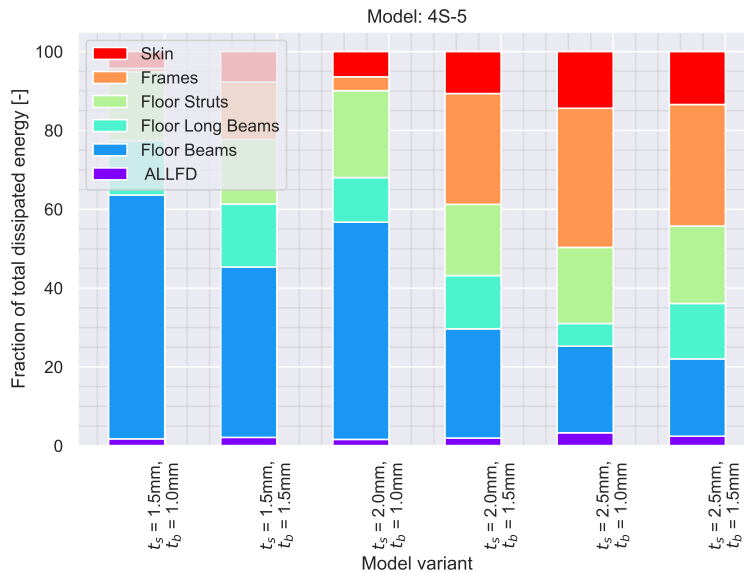

Fig. 9: Distribution of energy dissipated across components. ALLFD refers to energy dissipation due to friction. Configurations with thin floor struts dissipate more energy through deformation of the floor structure, whereas thicker struts cause more deformation at the frames.
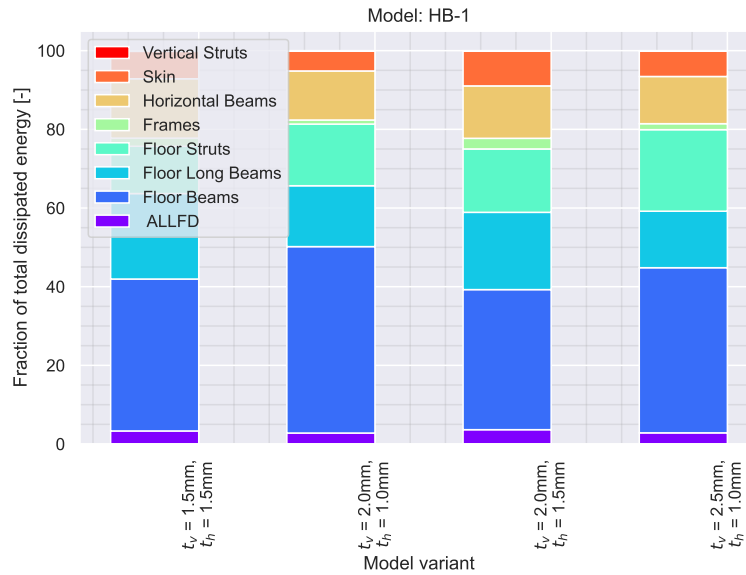
Fig. 10: Distribution of energy dissipated across components. Frames are contributing very little to energy absorption, due to lower load introduced by the floor struts, and most of the work is in turn being done by the floor structure. The vertical strut dissipates $\approx 0.1\%$ of the energy, and is thus not visible in the bar chart. ALLFD refers to energy dissipation due to friction.

2. HB Concept

The best configuration for the HB concept is HB-1, with a DRI of 22.2 units. Tab. 3 indicates that all HB configurations have approximately the same weight, except for HB-2 and HB-3, for which the crushable mass is 2% of the total section mass, due to the increased thickness of the floor struts and/or floor cross beam. The thicknesses of the crushable components, for the best variant of each HB configuration, as well as the pre- and post-crash sections can be visualized in Fig. B.3 and Fig. B.4. The initial intent of concept HB was to allow some deformation of the floor cross beam during the first phase of the crushing, as the horizontal beam that supports the vertical strut does not have high bending stiffness. For increasing displacement, the horizontal beam's loading will change from bending to tension, which increases its stiffness and will favor the crushing of the vertical strut. However, Fig. 10 indicates that the plastic deformation of the vertical strut is so little that it is in fact not visible in the graph. Data shows that it is hovering around 0.1%, depending on the variant. This is also visible in Fig. B.6, where the deformed sections' plastic strains contour plot indicates no plastic deformation of the vertical strut.

This is caused by the out-of-plane bending of the horizontal beam and the subsequent rotation of the entire assembly about the floor cross beam. This can be seen as structural instability: compared to tension, bending is a lower energy state and is thus the preferred deformation option.

A second observation is that the frames absorb little energy, compared to 6S and 4S concepts. In fact, $\approx 60\%$ of the dissipated energy is absorbed by the floor structure itself, thus, the loads are hardly transferred to the frames. Actually, this means that the frames are not able to even dissipate their own kinetic energy, thus, have an overall negative effect on the crash properties of the section: after the impact, the frames will rebound and, only during this phase, then, their kinetic energy is dissipated by other structural elements. Additionally, about 15-20% of the dissipated energy is absorbed by the floor struts, and only about 12-15% by the horizontal beams.

The thickness of the vertical strut has virtually no effect on the energy absorption (which is expected, considering that it does not plastically deform), while, regarding horizontal beams, an increase in thickness will cause the absorbed energy to overall slightly decrease: a stiffer horizontal beam will likely slow down the floor assembly by storing more elastic energy and, thus, when plastic deformation occurs, fewer kinetic energy will be dissipated plastically.

3. HBH Concept

The version with the lowest DRI for concept HBH is HBH-2 (24.4 units); as shown in Tab. 3, all HBH configurations have approximately the same mass. The normalized energy absorbed is presented in Fig. 11. In HBH, a similar structural instability as observed in concept HB is triggered. This is visible in Fig. B.5, where the pre- and post-crash sections are shown. While some crushing of the vertical struts does occur, this is limited and large parts of the plastic deformations occur in the horizontal beams, as also indicated by the data shown in Fig. 11.
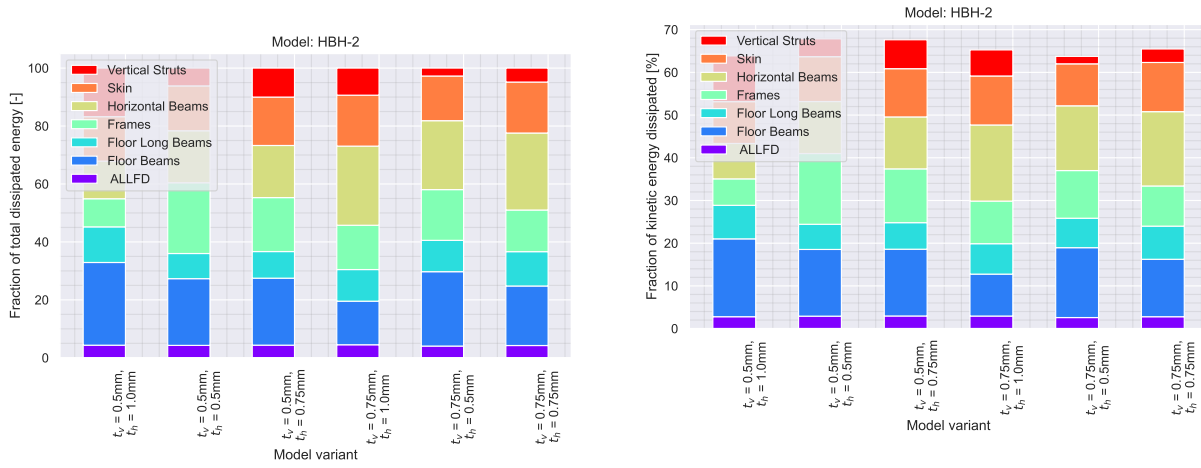
(a) Component energy absorption distribution, HBH-2 concept.

(b) Component energy absorption distribution, normalized by initial kinetic energy, HBH-2 concept.

Fig. 11: Distribution of energy dissipated across components. All variants are approximately able to dissipate similar amounts of energy. Struts with thinner walls show an improvement in energy absorption, while the opposite is true for the horizontal beams.

Regarding SEA, as shown in Tab. 3, it is clear how poorly effective the crash structure is at absorbing energy, if compared to concepts 6S, 4S, and most configurations of HB. The vertical struts and horizontal floor cross beams add a significant amount of additional structure, which, however, due to the instability, does not pay off. Fig. 11b shows that all variants approximately dissipate the same fraction of the pre-impact kinetic energy, while some variation in the contribution of the individual components. A general, obvious trend is observed, where lighter variants have higher SEA. Fig. 11b shows that all the variants are able to dissipate roughly the same percentage of initial kinetic energy. Clearly, then, lighter ones will have higher SEA.

Interestingly, compared to concept HB-1, as shown in Fig. 10, the frames are now absorbing a more significant portion of energy. In essence, before the structural instability is triggered, more load is transferred through the horizontal beams to the frames; this is further proven by the more significant portion of energy that is dissipated thru the horizontal beams, hovering about 20%, and less by the floor structure. As expected the vertical struts perform quite poorly, as they are in fact never crushed. The fraction of energy absorbed by the fuselage skin is in turn more similar to that of concepts 4S and 6S. As mentioned earlier in this article, the energy dissipated by the skin is closely related to that dissipated by the frames; this is thus consistent with that observation.

Overall, a trend can be hardly identified, due to the complexity of the observed failure mode. However, in general, the vertical struts seem to be performing best when thinner, while the opposite is true for the horizontal beams. This is logical as the structural instability is not caused by Euler buckling of the struts, but rather by out-of-plane displacement of the horizontal beams. Having a thinner wall for the vertical struts will allow them to deform before and during the instability occurs, while thicker horizontal beams will delay the aforementioned instability.

C. Discussion on the Results

First and foremost, it is worth noting that the crushable mass represents a small percentage of the fuselage section mass. This fraction becomes even smaller considering that floor cross beams have also been included in the determination of the crushable mass, the design of which is however determined not solely by crashworthiness requirements, but also by structural sizing constraints (as they contribute to keeping the oval shape of the pressurized fuselage). All in all,

differences in mass fractions across crash concepts will always be small. Despite that, crash performance is shown to change significantly.

From the data presented above, none of the explored concepts was able to meet the requirement of 16 DRI units. The best-performing one is 4S-5, with an equivalent DRI of 18.2 units. The main bottleneck is the lack of plastic deformation of the frames, which, in conventional aircraft, dissipate the vast majority of the kinetic energy.

Considering concepts 6S and 4S, it is concluded that, given the already high stiffness of the frames, it will not be beneficial for crashworthiness, to have a large number of floor struts. It is, instead, recommended to only consider designs employing four struts, in future studies.

Frames are a crucial element for crashworthiness and, as demonstrated in this study, for unconventional aircraft configuration their importance should not be overlooked. While their sizing will mostly be determined by operational loads, for future design iterations, it is fundamental to focus on the deformation of the frames to absorb energy. As proven by concepts HB and HBH, disregarding this aspect has not worked, at least within this research. Furthermore, it is worth emphasizing once again, at this point, that in the current research, the frames' geometry has been simplified significantly. The consequence of this is that, although on average the bending stiffness is kept approximately constant, it is however overestimated at the locations where plastic deformation occurs, in the vicinity of the floor struts anchor points. As shown in Dotman's research, this corresponds to the region where the actual frame height is quite low [4]. It is therefore likely that, if a more accurate model had been developed, the crash properties of the analyzed section would have improved significantly. This will be in part confirmed by the sensitivity analysis study, where the thickness of the frames is varied in order to check for the significance of the simplifications made. However, while it is true that in those critical regions, the frame stiffness is overestimated, it should be noted that in other regions, such as the center of the keel, it is underestimated. An increase in stiffness of the central part of the keel would prevent flattening of the lower portion of the frames, likely causing deformations that are completely different from those seen in conventional aircraft configurations. Accurate modeling of the section is thus left as a future study.

The unconventional HB and HBH concepts are poorly performing, as they are not able to dissipate large amounts of energy, and are prone to large rebounds as a consequence of that. In particular, HBH is highly subjected to structural instability. It has been mentioned, earlier in this report, that, since concepts HB and HBH are significantly more complex than 4S (and 6S).

In terms of overall deformations all concepts are subjected to large floor cross beam compliance, which is more limited in 4S and 6S where the cross beam is better supported by the floor struts, and this is significantly more pronounced in HB and HBH. Concepts HB and HBH were conceived to absorb energy by means of cross beam deformation, while a larger focus on the creation of plastic hinges at the frames was given for 4S and 6S. Furthermore, the large compressive load present in the floor struts of the latter concepts does mean that these struts are producing a stabilizing effect on the cross beams by limiting their deformation.

Having more compliance at the cross beams allows for an increase in the impact time, thus reducing the acceleration experienced by the passengers. Excessive deformations of these cross beams during crash, however, might damage the interior floor panels, and directly affect the post-crash volume, which could negatively affect passengers' evacuation. This is an especially unwanted result in light of recent proposals from US lawmakers, to create more stringent and real-life alike cabin egress requirements[4,5].

To summarize, the simulations herein performed show a clear direction for the design of a crashworthy Flying-V typical section, which calls for a conventional cross beam-and-struts approach; with localization of the loads at a single anchor point in order to achieve a plastic hinge on the frames. Some deformation of the cross beams will likely be beneficial when combined with requirements on the allowed deformation in order to favor the egress of the occupants from the cabin.

Lastly, a few considerations need to be made, regarding the limits of this current study:

- **Tail-impact first and rigid body rotation:** The current assessment of the crashworthiness of the Flying-V aircraft relies on currently accepted means of compliance by regulators, namely a simple drop test of the typical fuselage section. While this is a simple and traditionally effective method to assess aircraft crashworthiness, it also relies on the experience gained from decades of aviation history. Compared to conventional aircraft fuselages, the Flying-V is more rigid and stronger. As a reference, post-crash pictures of the Boeing 737 aircraft, show the fuselage to fracture in three distinct sections, after a crash-landing: one forwards of the central wingbox, one

---

[4]`https://www.chicagotribune.com/opinion/commentary/ct-opinion-faa-plane-evacuation-standards\-duckworth-20221230-leowchniknb2rd623xbgrhz7jm-story.html`. Accessed on 24-May-2023.

[5]`https://www.reuters.com/world/us/us-senators-want-faa-rewrite-aircraft-evacuation-standards\-2022-12-08/`. Accessed on 24-May-2023.

containing the central wingbox, and a tail section[6]. During a tail-impact first crash landing, it is possible for the Flying-V outer wings to be damaged and even separate from the main body, which would dissipate energy and directly affect its crashworthiness. However, the stiffer and stronger fuselage section would likely ungergo a significant amount of rigid-body rotation when the wing tipsstrike the ground, resulting in upwards forces that induce a strong pitch-down moment on the aircraft, and subsequent rotation. The front-most part of the cabin will thus have a higher vertical impact velocity than the aft part, resulting in higher accelerations experienced by the occupants in the front part. A proper evaluation of the Flying-V rigid-body dynamics has not been performed as part of this research, and will thus be left as a recommendation for future studies.

- **Fuel and sloshing:** the Flying-V aircraft will store fuel aft the wing-fuselage spar, in the trailing edge region. While it is unlikely that fuel will be stored in the tank in a wet structure configuration; the presence of fuel significantly increases the criticality of structural fractures happening at the wing-fuselage spar during crash. In current analyses, fuel mass has not been accounted for due to lack of data. Once again, this is left for future studies. However, besides the fuel mass, a critical factor that might emerge is damage caused by the sloshing of the fuel itself, after the impact. The accident investigation following the tragic accident of the Aérospatiale/BAC Concorde of 2001, determined that the root cause of the damage to the fuel tank of the aircraft was not the direct impact of tire debris, but the shock wave triggered by the impact and the subsequent pressure surge [18]. Considering the vicinity of the passengers to the fuel tanks in the Flying-V aircraft, it will be of prime importance to ensure reliable separation of the fuel from the cabin, even during higher-speed impacts that must be still survivable. As such, it is recommended for future studies to include the interaction between fuel sloshing and the structure during a crash landing, for different amounts of stored fuel. Moreover, it is recommended to include bulkheads in fuel tanks, at the location where the Flying-V wing-fuselage is likely to fracture into separate sections, to ensure that even in such an event the fuel can be still contained.
- **Seat orientation:** in the FV, as opposed to conventional aircraft, passenger seats will not be aligned with the direction of flight, but rather with an angle of 18 deg, which is the maximum allowed for the use of conventional belts as specified in CS 25.785 [16]. This will likely result in the introduction of side loads on the passengers, which are generally unaccounted for during vertical drop tests. The influence of said side loads on the results herein presented is unknown and it is recommended to be the subject of further studies.

V. Sensitivity Analysis

The preliminary assessment on the crashworthiness of the Flying-V aircraft presented in the previous section is based on the model of a fuselage section which relied on some simplifications and assumptions required to reduce the modeling and simulation times. However, such simplifications had an effect on the results, and the main goal of this sensitivity analysis is to map the effects of the following parameters:

- Mesh size
- Floor cross beams thickness
- Floor cross beams flange width-to-web height ratio
- Floor struts thickness
- Floor struts flange width-to-web height ratio
- Frames thickness

The reasons for the choice of each of the aforementioned parameters will be discussed in the relevant subsection.

Almost all variants are contained within a narrow band with DRI ranging between 18 and 19, and the fraction of absorbed energy between 70% and 73%, indicating that small variations in thickness and web-to-flange dimension ratios do not have a large effect on the crash properties. The three exceptions to this are the two variants tested with different frame thicknesses, and one with a thinner cross beam, as visible from Fig. 12.

A. Mesh Size

Compared to the F-28 Fellowship section used for validation purposes, the overall size of the structure is obviously increased since the Flying-V is a much larger aircraft; as such, the element size for all the structural elements, for the Flying-V section is kept the same at best, if not decreased, in order to have sufficient confidence in the accuracy of the analyses. The first sensitivity analysis consists of a mesh convergence study starting with the mesh sizes shown in Tab. 1

---

[6]https://christinenegroni.com/boeing-workers-warn-of-737-ng-structural-problems-then-4\-planes-fracture/. Accessed on 24-May-2023.
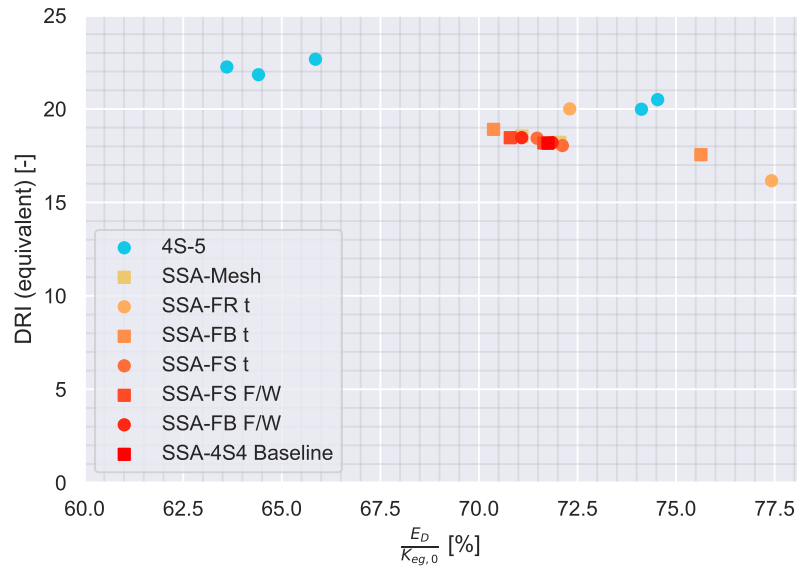
Fig. 12: Comparison between 4S-5 concept variants and sensitivity analysis models. Overall, large differences in DRI and energy-absorption levels can be observed to be mainly occurring for variations in frames and cross beam thicknesses. Other quantities have a smaller effect.

as baseline, and successively refining it so that the global element size would be that of the baseline, multiplied by a factor of 0.9 and 0.8.

The results are tabulated in Tab. 4, and further presented in Fig. 13 and Fig. 14. Pictures of the deformed sections are provided in Appendix B.

Tab. 4: Comparison of DRI, kinetic energy dissipated, and SEA for different mesh refinement levels. All metrics show good agreement with the baseline mesh size, giving confidence on the accuracy of the solution.

Version	DRI [-]	$\frac{E_D}{K_{EG}}$ [%]	SEA [kJ/kg]
Baseline	18.2	72	1.47
0.9x mesh size	18.2	72	1.46
0.8x mesh size	18.5	71	1.45

The baseline model consists of 178947 elements and 193896 nodes. In the 0.9x model, the number of elements increased to 217246, corresponding to a total of 233948 nodes. Lastly, the 0.8x model has 272197 elements and 290789 nodes. The skin is excluded from the mesh refinement, assuming that it will not undergo complex deformations other than plastic bending.

The convergence analysis shows an overall slight decrease in energy absorption (and, thus, SEA), which is nevertheless <2% and thus considered negligible. The most significant difference is the increase in the equivalent DRI measured from 18.2 units to 18.5 units, which corresponds to an increase in the probability of spinal injury from 12.5% to 15.7%. This is likely due to the increase in the crippling load of the floor struts associated with a more refined mesh. Overall, this convergence analysis provides confidence that the results determined with the 'baseline' mesh size are sufficiently accurate and trustworthy.

Fig. 13: SEA for mesh sensitivity analysis variants. All models have almost identical SEA.
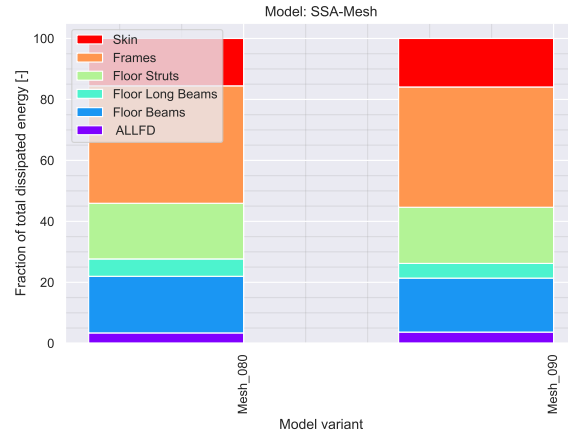
Fig. 14: Energy absorption distribution by component, mesh sensitivity analysis. No significant variations are noted, for different mesh refinement levels. The '080' and '090' values denote a global element size equal to 0.80x and 0.90x that of the baseline, respectively.

B. Floor Cross Beams Geometric Parameters

As mentioned in the introduction section, two distinct cross beam geometric parameters are chosen for the sensitivity analysis, being the thickness and the ratio between the beam's web height and flange width. The results are presented in the current subsection.

1. Cross Beam Thickness

Starting with the analysis of the cross beam thicknesses, it is found that a thinner cross beam is highly beneficial for crashworthiness. A thinner cross beam deforms more, absorbs more energy, decreases loads on the occupants, and decreases the crushable mass, causing a large increase in SEA, as evident from Tab. 5 and Fig. 15. As more energy is absorbed by the cross beam itself, the frames become less loaded, thus contributing less to the overall energy absorption. On the other hand, the energy fraction absorbed by the floor struts remains approximately constant, as their bucking and crippling loads are less sensitive to the thickness than to the strut cross section geometry, as shown in Fig. 16.

It is worth noticing, however, that although not specified in the context of this research, a requirement on the maximum allowed bending of the passenger cross beam must be set, considering the high sensitivity of the crash characteristics to the thickness of the cross beam. Excessive deformations of the cross beam must be avoided, as it would impede occupant egress in the event of a crash.

Tab. 5: Comparison of DRI, kinetic energy dissipated, and SEA for different cross beam thicknesses. All metrics show how thinner cross beams can significantly reduce DRI and energy absorption levels. This, however, comes with the penalty of significant cross beam deformation.

Version	DRI [-]	$\frac{E_D}{K_{EG}}$ [%]	SEA [kJ/kg]
t_b =0.75 mm	17.6	76	1.82
t_b =1.0 mm (baseline)	18.2	72	1.47
t_b =1.25 mm	18.9	70	1.25
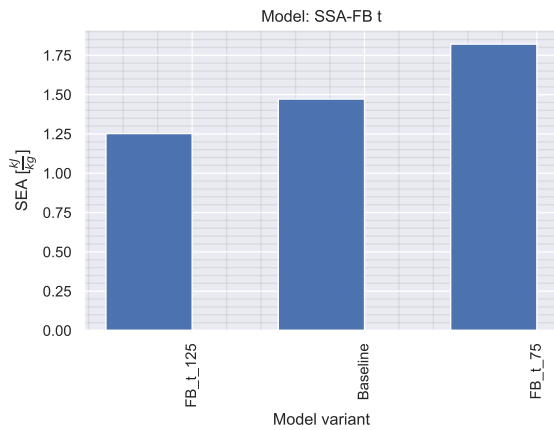
Fig. 15: SEA for cross beam thickness sensitivity analysis. SEA increases for thinner cross beams due to 1) lighter beams and 2) an increase in energy absorption.
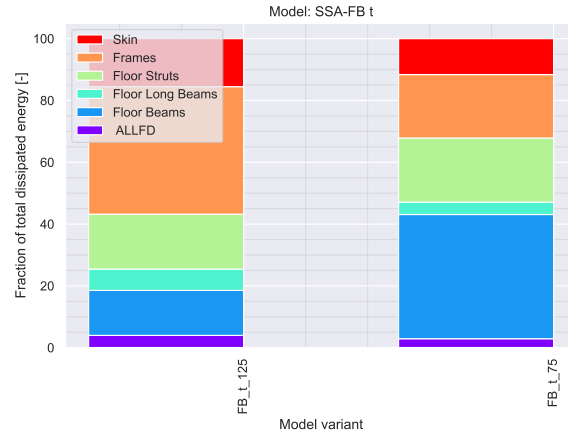
Fig. 16: Energy absorption distribution by component, cross beam thickness sensitivity analysis. The energy absorbed by the cross beams increases significantly as they become thinner.

2. Cross Beam Flange Width-to-Web Height Ratio

The cross beams have an I-shaped cross-section with a web height-to-flange width ratio equal to 3. It is of interest to check whether different ratios would have a positive, negative, or neutral effect on the crash properties. The hypothesis is that variants with lower ratios are more stable showing no lateral torsional buckling {LTB} with an increase of the flange width. In order to isolate other variables, it is decided to keep the beam's flexural rigidity constant in the sensitivity analysis. As the width of the flanges with respect to the web height increase, then the height of the beam's web needs to be decreased to keep the same flexural rigidity. Using the thin-walled approximation, (6) can be derived, which allows determining the new I-shaped beam height as a function of the old beam height, and the respective flange width-to-web height ratios, keeping the flexural rigidity constant:

$$h_2 = h_1 \left(\frac{\frac{1}{12} + \frac{n_1}{2}}{\frac{1}{12} + \frac{n_2}{2}} \right)^{\frac{1}{3}} \tag{6}$$

where h_1 and h_2 are the old and new beam heights, while n_1 and n_2 are respectively the old and new flange width-to-web height ratios. For the baseline variant, $n_1 = \frac{1}{3}$, resulting in a cross beam web height of 209 mm for $n = \frac{1}{2}$ and $h = 244$mm, for $n = \frac{1}{4}$. As mentioned earlier, $h = 230$mm for $n = \frac{1}{3}$.

The sensitivity analysis data is presented in Tab. 6, Fig. 17 and Fig. 18. For consistency with the plots, in Tab. 6, the variants are denoted using the inverse of n.

Tab. 6: Comparison of DRI, kinetic energy dissipated, and SEA for different ratios of cross beam web height-to-flange width. Within the analyzed range, no significant differences are noted.

Version	DRI [-]	$\frac{E_D}{K_{EG}}$ [%]	SEA [kJ/kg]
FB $\frac{F_w}{W_h} = 2$	18.5	71	1.38
FB $\frac{F_w}{W_h} = 3$ (baseline)	18.2	72	1.47
FB $\frac{F_w}{W_h} = 4$	18.2	72	1.48

Data shows that the ratio of the flange-to-web dimensions has in fact little effect on the crash properties, within the examined range. Likely this will differ for more extreme configurations. The energy absorption distribution by components, shown in Fig. 18, are essentially unaffected, as well as the total absorbed energy, as given in Tab. 6. An increase in SEA for variants with higher $\frac{F_w}{W_h}$ is noted, which is attributed to the natural lightening of the cross beam
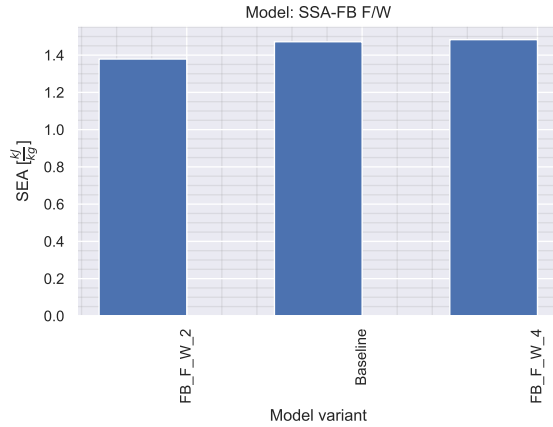
Fig. 17: SEA for cross beam height-to-width ratio sensitivity analysis. SEA only slightly increases for larger ratios since, when keeping flexural rigidity constant, the cross beam becomes lighter for higher ratios.
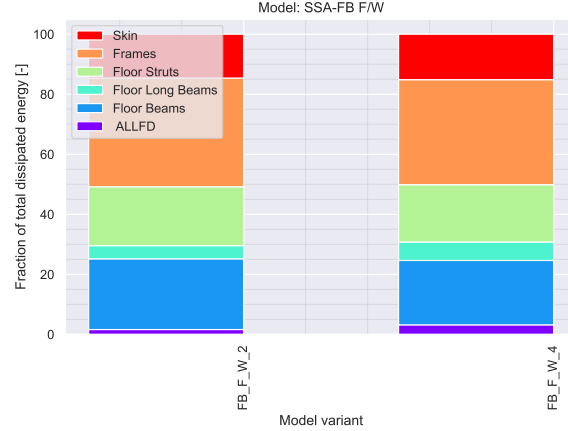
Fig. 18: Energy absorption distribution by component, cross beam height-to-width ratio sensitivity analysis. Within the analyzed range, a changing ratio has little to no effect.

when the height is increased and the flexural rigidity is kept constant, as it is more efficient to place material further away from the neutral axis. Lastly, an increase in DRI is noted for the variant with the lowest $\frac{F_w}{W_h}$, which is likely because, although the beam's second moment of area is constant, the height is decreased, leading to lower stresses and, thus, reduced buckling.

C. Floor Struts Geometric Parameters

Regarding the floor struts, a similar sensitivity analysis is performed compared to the cross beams, changing the thickness and the ratio between the struts' web height and flange width.

1. Floor Struts Thickness

Starting with the thickness of the floor struts, the results show that the energy absorbed remains approximately unchanged. As evident from Fig. 20, in variants with thicker floor struts, the frames are able to absorb a bit more energy. On the other hand, the floor structure is subjected to fewer plastic deformation. Consequently, SEA is higher for thinner struts, as the crushable structure becomes lighter (Fig. 19).

Tab. 7: Comparison of DRI, kinetic energy dissipated, and SEA for small variations in floor struts thickness. Thinner floor struts allow for greater cross beam deformation, thus, lowering the DRI while still allowing the structure to absorb the same amount of energy.

Version	DRI [-]	$\frac{E_D}{K_{EG}}$ [%]	SEA [kJ/kg]
t_s =2.25 mm	18.0	72	1.55
t_s =2.50 mm (baseline)	18.2	72	1.47
t_s =2.75 mm	18.4	71	1.41

In terms of accelerations, an increase in floor struts thickness results in an increase of DRI (Tab. 7) as thicker floor struts limit the flexure of the cross beam.

2. Floor Struts Flange Width-to-Web Height Ratio

Regarding the floor struts' flange width-to-web height ratio, similar to what is done for the cross beams, it is decided to keep the flexural stiffness constant when changing the ratio. As the floor struts buckle during the crash, it is decided
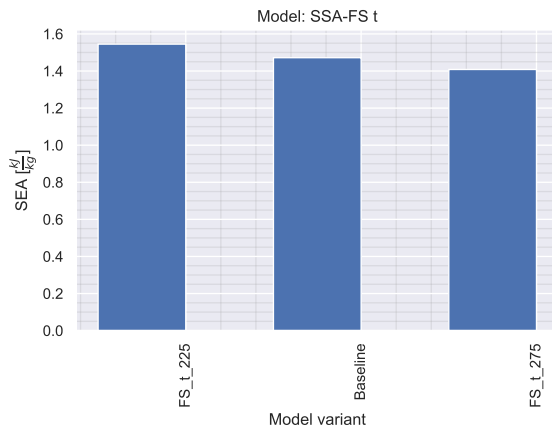
Fig. 19: SEA for floor struts thickness sensitivity analysis. A slight decrease in SEA is attributed to heavier crushable mass, due to the increase in struts thickness.
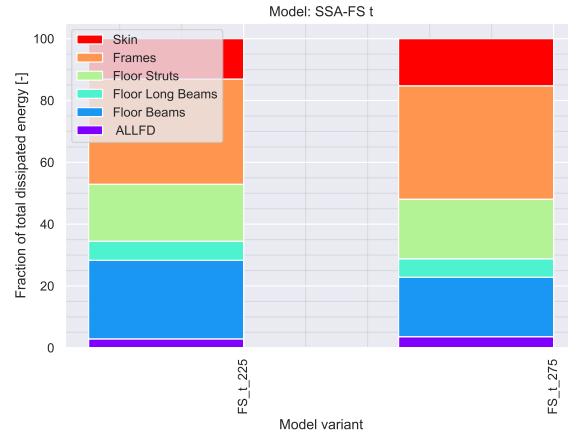
Fig. 20: Energy absorption distribution by component, cross beam thickness sensitivity analysis. Small variations in floor struts thickness have little to no effect on the energy-absorption characteristics.

to keep constant the flexural rigidity about the minor axis, i.e. the axis about which I_{xx} is the lowest. In a C-section, this corresponds to that which is parallel to the web. Again, using the thin-walled approximation, (7) was derived, linking the web heights of C-sections with different flange width-to-web height ratios.

$$h_2 = h_1 \left(\frac{\frac{n_1^3}{6} + 2\frac{n_1^3}{(4n_1+2)^2} + \frac{n_1^4}{(2n_1+1)^2}}{\frac{n_2^3}{6} + 2\frac{n_2^3}{(4n_2+2)^2} + \frac{n_2^4}{(2n_2+1)^2}} \right)^{\frac{1}{3}} \tag{7}$$

The parameters h_i and n_i are the same as those presented for (6), resulting in $h = 32$mm for $n = 1$, and $h = 87$mm for $n = \frac{1}{3}$. For the baseline configuration: $h = 60$mm and $n = \frac{1}{2}$. The results are presented in Tab. 8, Fig. 21, and Fig. 22.

Tab. 8: Comparison of DRI, dissipated kinetic energy, and SEA for different floor struts flange width-to-web height ratios. Cross beams with width-to-height ratios closer to 1, within the analyzed range, tend to be more flexible, and thus have lower DRI.

Version	DRI [-]	$\frac{E_D}{K_{EG}}$ [%]	SEA [kJ/kg]
FS $\frac{F_w}{W_h} = 1$	17.9	73	1.59
FS $\frac{F_w}{W_h} = 2$ (baseline)	18.2	72	1.47
FS $\frac{F_w}{W_h} = 3$	18.1	72	1.37

The sensitivity analysis data is consistent with what is expected and found earlier in the crash simulations. Floor struts with a 1:1 ratio between the web and the dimensions of the flanges tend to have more similar flexural rigidity about the two principal axes. As the ratio increases, since the stiffness about the minor axis is kept the same, then the second moment of area about the major axis increases. Overall, consequently, the floor strut becomes stiffer. Indeed, as shown in Fig. B.1, floor struts do purely buckle only about their minor axis, but also twist. The twisting motion is affected by the stiffness about both principal axes, and not only the minor one. Note that $J = I_{xx} + I_{yy}$ [19], with J being the polar second moment of area.

In short, floor struts in variants with values of n closer to 1 and smaller than 1, are more flexible. As seen earlier, more flexible struts allow for lower DRIs, as more energy is absorbed by the floor structure. This trend can be observed by Fig. 18. Lastly, regarding SEA, it is higher as floor struts in variants with n closer to 1 are lighter.
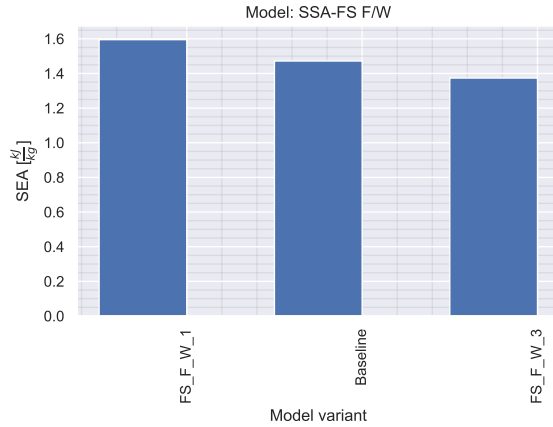
Fig. 21: SEA for floor struts height-to-width ratio sensitivity analysis. A decrease in SEA is associated with an increase in crushable mass, for larger web height-to-flange width ratios
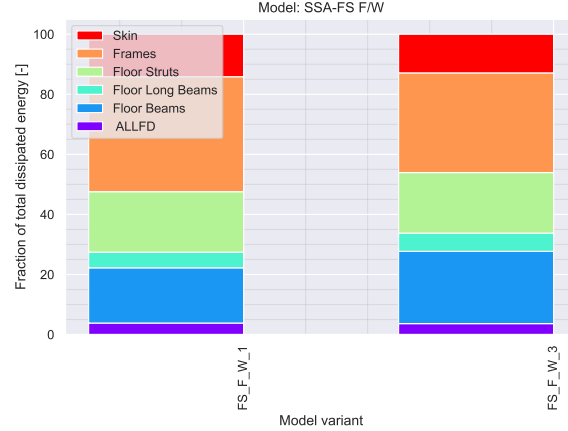
Fig. 22: Energy absorption distribution by component, floor struts height-to-width ratio sensitivity analysis. No significant changes in the energy absorption distribution can be observed.

D. Frames Thickness

Lastly, a sensitivity analysis on the frames' thickness is performed. Data is tabulated in Tab. 9, and further presented in Fig. 24 and Fig. 25. The results show that, above all, the frames' thickness and consequently the frames' bending stiffness have a large impact on the crash behaviour of the Flying-V. This is of particular importance since one of the early modeling assumptions was to keep the frames' height and thickness constant with respect to Dotman's [4] design. The results of this sensitivity analysis show that this simplification is overly-conservative, and that higher fidelity models considering the variable thickness and height will likely render better crash characteristics.

Assuming that the bending stiffness varies linearly with the shell thickness, which is reasonable when using the thin-walled approximation, then a 30% reduction in bending stiffness from 6.7 mm to 4.7 mm, considering the two external versions, would results in a significant DRI decrease of 4 units. In theory, such reduction translates to a reduction on the risk of spinal injury from approximately 30% to just over 3%. As mentioned in section IV, a DRI of 16 is generally accepted for certification purposes.

Tab. 9: Comparison of DRI, kinetic energy dissipated, and SEA for variations in fuselage frames thickness. It is likely that in the current research, the frame bending stiffness is overestimated in critical locations, leading to overly-conservative results. By reducing the frame bending stiffness, DRI can be significantly reduced. SEA does not increase in version with thinner frames since, for concept evaluating purposes, and frames are not included in the calculation of the crushable mass.

Version	DRI [-]	$\frac{E_D}{K_{EG}}$ [%]	SEA [kJ/kg]
$t_{FR} = 4.7$mm	16.2	77	1.53
$t_{FR} = 5.7$mm (baseline)	18.2	72	1.47
$t_{FR} = 6.7$mm	20	72	1.52

The decrease in DRI is the result of a softer impact caused by a significant plastic deformation of the frames, which is highly desired in aicraft crashworthiness. Fig. 23 shows the deformed section of the variant with 4.70 mm frames thickness.

From inspection of the crashed section, a significant rotation of the frames is evident, with a flattening crushing behavior. In conventional aircraft configurations, the bending stiffness of the frames and that of the floor struts are of a comparable order of magnitude. As a consequence, the floor struts are more able to influence the deformation pattern of the frames, which is supported by physical and virtual tests from the literature that show the floor struts dictating the
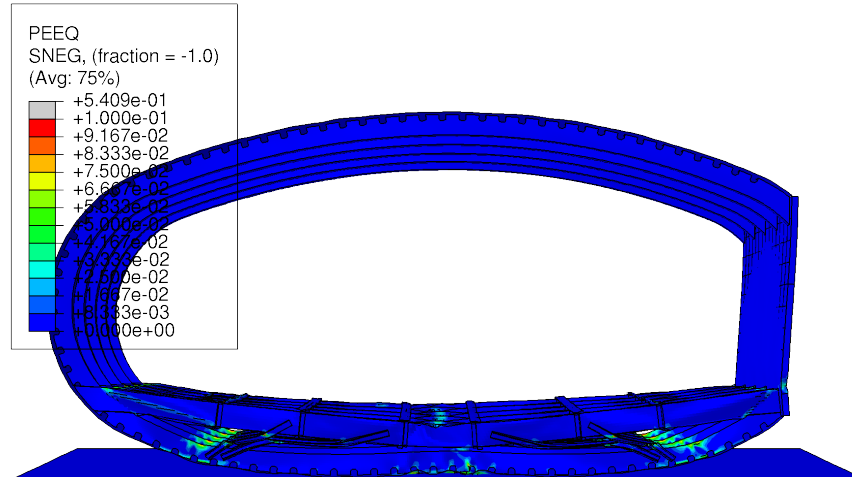
Fig. 23: Fuselage section with thinner frames, post-crash. PEEQ is the keyword used by Abauqs to denote the equivalent plastic strain. The frames are able to deform significantly, showing a flattening crashing behavior.

location of the plastic hinges on the frames [5, 20–22]). For the Flying-V, as herein investigated the opposite happens: the frames are significantly stiffer than the struts and, as a consequence, when the frames deform the floor struts are dragged by them. This means that, when the frames deform, a significant bending load is introduced in the floor struts which, subsequently, buckle prematurely. An increase in the thickness of the floor struts and overall dimensions might be able to further allow the creation of a plastic hinge on the frame, while providing a better support to the floor cross beams.
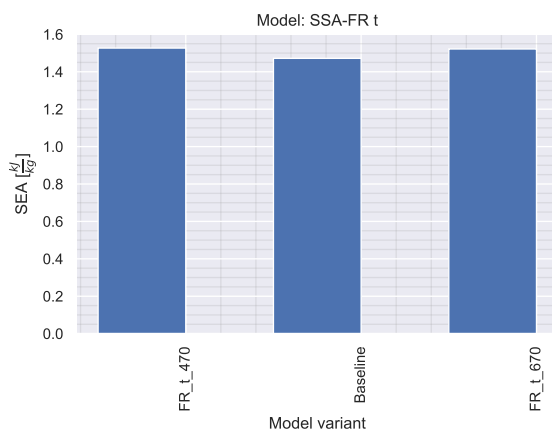
Fig. 24: SEA for thickness sensitivity analysis. Although thinner frames absorb significantly more energy, no variation in SEA is observed as the frames are not included in the calculation of the crushable mass.
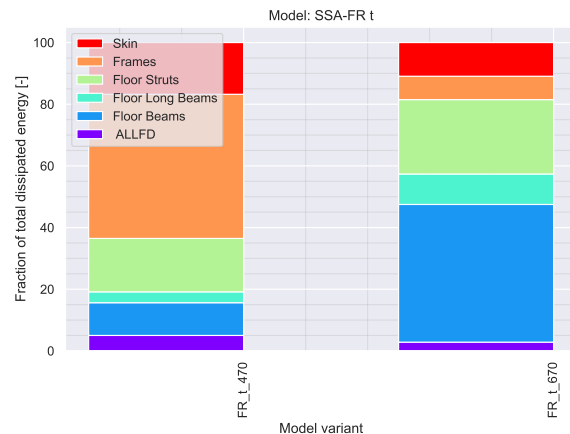
Fig. 25: Energy absorption distribution by component, frames thickness sensitivity analysis. The frames' bending stiffness has a significant impact on the energy-absorption characteristics of the section.

Considering Fig. 24, SEA only slightly increases for the thinner frames variant, since the mass of the frames are not included in the calculation of the crushable mass. Additionally, Fig. 25 clearly shows that the frames' thickness plays a crucial role on how the different structural components absorb energy.

Lastly, some plastic deformation of the spar occurs. As mentioned earlier, sizing of the currently chosen concept of the wing-fuselage orthogrid spar has not been performed yet, making it unknown whether the assumed spar orthogrid

parameters are conservative or not. The plastic energy dissipated by the wing-fuselage spar is not shown in Fig. 25, as for all previously tested variants, no plastic deformation of the spar plates occurred, such that the plastic deformation energy output for the spar is not requested from Abaqus' explicit solver. Regardless, these results highlight an important aspect regarding the crashworthiness of the Flying-V: fire. The fuel tanks are located next and alongside the passenger's cabin, separated by the wing-fuselage spar. Fig. 23 clearly shows that the high impact forces are able to bend the spar, and even possibly fracture it. By design, this should be avoided and the consequences mitigated. Although, in all likelihood, fuel will be stored in a bladder, fracture of the wing-fuselage spar during a crash event might puncture the bladder itself, creating a direct and hazardous flow path between the fuel tanks and the passenger cabin.

E. Discussion on the Results

Results from the mesh convergence analysis show that, in terms of finite element size, little to no variation is present between the baseline and the refined models, with the greatest difference being an increase in DRI of 0.3 units. This is attributed to the highest crippling resistance associated with a more refined mesh, giving good confidence that the adopted baseline model is sufficiently converged.

Regarding the floor struts and cross beams, the ratio between the web height and flange widths of the beams has a limited effect on the crash and energy-absorption capabilities of the fuselage section, as the second moment of area about the major axis is kept constant. Changing ratios without fixing the flexural rigidity of the beam would certainly affect the crash behavior. Such high sensitivity is demonstrated by the fact that the crash results are largely affected by small variations in cross beam thickness, whereas affected to a lesser extent by small variations in struts thickness; and these variations in thickness have a direct effect on the beam's flexural rigidity.

More flexible structures, and, in particular, flexible cross beams, have a significantly beneficial effect on the DRI. While in the results presented in section IV the variations are as large as 0.5 mm, this value has been halved for the sensitivity analysis, still leading tosignificant variations in DRI and energy-absorption capabilities. It is worth emphasizing that, for cabin egress reasons, the deflection of the cross beams should be further limited. Moreover, the cross beam also plays an active role in keeping the Flying-V fuselage shape during pressurization cycles, a requirement that might lead to stiffer cross beam designs. Eventually, a final design shall be able to satisfy both requirements.

Furthermore, the sensitivity analysis on the frames' thickness gives good confidence that, in the future, it will be possible to design a crashworthy Flying-V fuselage section. In the current study, the frame bending stiffness is largely overestimated in crucial areas where a plastic hinge would be created, thus making the frames act as springs rather than energy absorbers under vertical drop test conditions. With reduced frame thickness, their energy-absorption capabilities significantly increase. In future design iterations, crashworthiness requirements will likely influence the frame bending stiffness distribution, and that of other structural components of the section. It is possible, for instance, that a reduced bending stiffness of the frames can be traded off for stiffer cross beams, especially if, as mentioned earlier, a requirement on their maximum deflection is to be set.

Lastly, it is evident from visual inspection of the post-crash section that large plastic strains are transmitted to the spar. Since no precise sizing data about the wing-fuselage spar for this configuration is available, is is likely that the wing-fuselage spar strength has been only roughly estimated. On the other hand, considering that this spar is an important separation barrier between the fuel tanks and the cabin, a proper analysis need to be performed in order to ensure that either the spar does not crack due to the local loads introduced by the connection with the frames, or that separation of the frames from the spar can occur before the spar itself is damaged.

VI. Conclusions and Recommendations

The most suitable crash concept identified within the present investigation on the crash behavior of the Flying-V concept was inspired on a more conventional layout, where two floor struts were placed underneath the floor cross beam. An unsuccessful placement of the floor struts resulted in little plastic deformation of the frames, large rebounds, and consequently high DRIs. Hence, the struts had to be optimally placed such that the frames could reach satisfactory levels of plastic deformation, dissipating energy and limiting the post-crash rebound, both factors contributing to lower the loads experienced by the occupants. However, a good degree of rigidity is still required to achieve plastic deformations, as an excessively flexible floor structure prolongs the impact time, lowering peak loads and resulting in overall lower plastic deformation levels.

Current results from the sensitivity analyses show that a thickness variations of ±0.25 mm for the floor cross beams and struts have little effect on the crash properties. The same result is achieved when the cross beam and struts' web-height to flange width ratio are changed by ±1 unit. Most interestingly, the sensitivity analysis shows that the

constant thickness and height simplification of the frame did have a large effect on the DRI, being therefore a constraint to be relaxed in future studies. This highlights the influence of the frames in the crashworthiness of unconventional aircraft configurations, especially in oval fuselage cross sections where the bending stiffness of the frames is significantly larger than those in conventional aircraft with circular cross sections. This larger bending stiffness comes from the deformations created under pressurization loads, and suggests that crashworthiness requirements should be considered during the sizing of the frames.

According to the DRI levels, the current research could not reach a crashworthy design for the typical section of the Flying-V. However, with the acquired data and experience our research group is now able to focus on combining airworthiness and crashworthiness requirements into a simultaneous layout and sizing optimization framework, which will enable further exploration of the design space. With such framework, we want to study the trade-off between weight, deformations in the oval fuselage section under pressurization loads, and DRI levels. The recommended structural concept to be pursued in future work is the 4S, given its current DRI performance and relative simplicity in terms of manufacturing and design.

References

[1] Benad, J., "The Flying V - A new Aircraft Configuration for Commercial Passenger Transport," *Deutscher Luft- und Raumfahrtkongress*, 2015. URL `https://www.dglr.de/publikationen/2015/370094.pdf`.

[2] Oosterom, W. J., *Flying-V Family Design (MSc thesis)*, 2021.

[3] Chen, S. Y., van de Waerdt, W., and Castro, S. G., "Design for bird strike crashworthiness using a building block approach applied to the Flying-V aircraft," *Heliyon*, Vol. 9, No. 4, 2023, p. e14723. https://doi.org/10.1016/J.HELIYON.2023.E14723.

[4] Dotman, T. P., *A Structural Sizing Methodology for the Wing-Fuselage of the Flying-V (M.Sc. Thesis)*, Delft, 2021.

[5] Gransden, D. I., and Alderliesten, R., "Development of a finite element model for comparing metal and composite fuselage section drop testing," *International Journal of Crashworthiness*, Vol. 22, No. 4, 2017, pp. 401–414. https://doi.org/10.1080/13588265.2016.1273987.

[6] Dassault Systèmes, "ABAQUS Documentation," , 3 2006.

[7] Kay, G., "Failure Modeling of Titanium 6Al-4V and Aluminum 2024-T3 With the Johnson-Cook Material Model," Tech. rep., Federal Aviation Administration, Washington DC, USA, 9 2003.

[8] Lyle, K. H., Stockwell, A. E., and Hardy, R. C., "Application of Probability Methods to Assess Airframe Crash Modeling Uncertainty," *Journal of Aircraft*, Vol. 44, No. 5, 2007, pp. 1568–1573. https://doi.org/10.2514/1.27722.

[9] Jackson, K. E., Littell, J. D., Annett, M. S., and Haskin, I. M., "Finite Element Simulations of Two Vertical Drop Tests of F-28 Fuselage Sections," Tech. rep., NASA Langley Research Center, Hampton, Virginia, USA, 2 2018. URL http://www.sti.nasa.gov.

[10] Alan Poston, "Human Engineering Design Data Digest," Tech. rep., United States Department of Defence, Washington, DC, 4 2000.

[11] Alfaro-Bou, E., Fasanella, E. L., and Williams, M. S., "Crashworthy Design Considerations for General Aviation Seats," *SAE Transactions*, Vol. 94, 1985, pp. 438–451.

[12] Brinkley, J. W., and Shaffer, J. T., "Dynamic Simulation Techniques for the Design of Escape Systems: Current Applications and Future Air Force Requirements," Tech. rep., Aerospace Medical Research Laboratory - Wright-Patterson Air Force Base, Dayton, Ohio, 12 1971.

[13] Coltman, J. W., Van Ingen, C., Johnson, N. B., and Zimmermann, R. E., "Aircraft Crash Survival Design Guide: Volume II - Aircraft Design Crash Impact Conditions and Human Tolerance," Tech. rep., Simula Inc., Phoenix, Airzona, 12 1989.

[14] Payne, P. R., and Stech, E. L., "Dynamic Models of the Human Body," Tech. rep., Aerospace Medical Research Laboratory - Wright-Patterson Air Force Base, Englewood, Colorado, 11 1969.

[15] Transport Aircraft Crashworthiness and Ditching Working Group, "Transport Aircraft Crashworthiness and Ditching Working Group Report to FAA (Rev. B)," Tech. rep., 10 2018.

[16] European Union Aviation Safety Agency, "Certification Specifications and Acceptable Means of Compliance for Large Aeroplanes (CS-25) - Amendment 27," , 2021.

[17] Federal Aviation Administration, "Part 25 - Airworthiness Standards: Transport Category Airplanes," , 2022.

[18] BEA, "Accident on 25 July 2000 at La Patte d'Oie in Gonesse (95) to the Concorde registered F-BTSC operated by Air France," Tech. rep., Bureau Enquêtes-Accidents, 2000.

[19] Megson, T., *Aircraft Structures for engineering students*, 6th ed., Butterworth-Heinemann, 2017.

[20] Xue, P., Ding, L., Qiao, F., and Yu, X., "Crashworthiness study of a civil aircraft fuselage section," *Latin American Journal of Solids and Structures*, Vol. 11, No. 9, 2014, pp. 1615–1627. https://doi.org/10.1590/S1679-78252014000900007.

[21] Lützenburger, M., "Studies about the Utilisation of the Aircraft Cargo Compartment as Additional Passenger Cabin by use of Numerical Crash Simulation," *The Fifth Triennial International Fire & Cabin Safety Research Conference*, 2007.

[22] Yu, Z. L., and Xue, P., "Crashworthiness study of composite fuselage section," *Key Engineering Materials*, Vol. 725 KEM, Trans Tech Publications Ltd, 2017, pp. 94–98. https://doi.org/10.4028/www.scientific.net/KEM.725.94.

Appendices

A. Model Validation

The FE simulations are validated by comparison with the mean accelerations at accelerometers locations reported in Fig. A.2. The results are shown in Fig. A.3, where the data from Fig. A.2 is digitized for the sake of clarity. For model validation, the mean acceleration at each accelerometer location for the 4 frames, friction model (in purple) is compared with NASA's drop test and simulation (upper and lower bound) results.
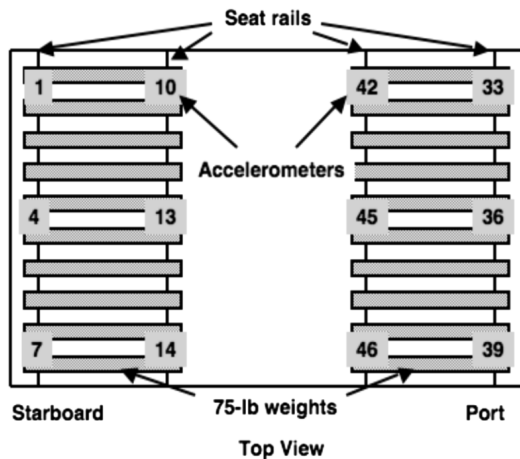
Fig. A.1: Schematic of fuselage section floor, and selected accelerometer locations and IDs [8].
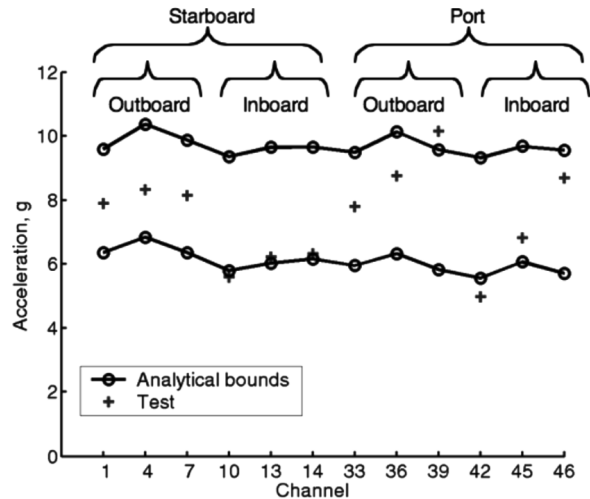
Fig. A.2: Comparison between probabilistic analysis bounds for the finite element analysis, and physical test results [8].

There is good agreement found between the physical drop test and the simulation results. The mean acceleration levels determined in the current work are on the higher end of the spectrum, as compared to the numerical upper bound determined by NASA's simulation. The main reason for this is likely that, since the structural components' dimensions, in particular thicknesses, have been determined by measuring the actual dimensions of the fuselage section in possession of TU Delft, then it is not physically possible to underestimate the thicknesses; thus, all measured thicknesses are accurate at best, and likely overestimated, thus resulting in an overall increase in stiffness of the fuselage section. Lastly, Fig. A.4 compares the after-impact state of the fuselage section with that of NASA's physical drop test and simulation. Once again, a good agreement is found between the three deformed shapes, in particular when comparing the two simulations.

Considering all of the above, the numerical model is validated.

Minimum Fuselage Section Size for Modeling

The final step towards the development of a validated FEA model to assess the crashworthiness of the Flying-V consists of the definition of the minimum fuselage section size that needs to be analyzed. As mentioned, in general, for certification purposes a six-frame section is used. Subsequently, it is decided to investigate if in fact a shorter section could be analyzed in order to reduce the size and computational cost of the model.

The data is presented in Fig. A.5.

Clearly, the difference between the three different sections is negligible. From visual inspection of the results, a reduction in the coupling between the crushing and twisting behavior of the fuselage section can be noticed. The twisting motion originates from the up-folding frames hitting the central floor longitudinal beam. Due to the asymmetrical cross-section of such a beam, the frames are deflected sideways, creating a crush-twist coupled motion. Longer sections show an increased stability against this crush-twist coupling.

To conclude, the difference in behavior between the three tested sections is small, such that the five-frame section is used to assess the crashworthiness of the Flying-V. The main reason is that, from visual inspection of the results, although this is not captured by the data presented in Fig. A.2 and Fig. A.5, the crushing-twisting motion observed in the four-frame section was significantly larger than for the other two.
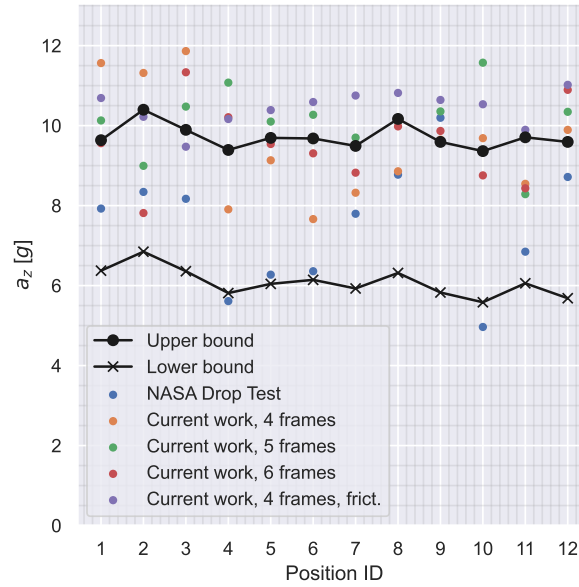
Fig. A.3: Comparison of mean acceleration values between NASA's F-28 drop test and simulation results [8], and current work. The position IDs 1 thru 12 correspond to those shown in Fig. A.1, in ascending order. The following observations can be made: 1) the measured accelerations for the 4 frames section are in line with those expected from NASA's study; 2) The introduction of friction reduces scatter in measured accelerations; 3) no fundamental differences can be observed between sections with different number of frames.
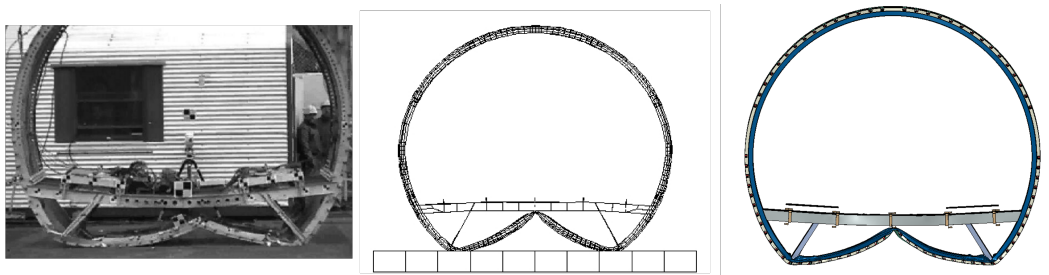
Fig. A.4: Side-to-side comparison between NASA drop test and simulations (left and middle), and current work (right). Adapted from [8].
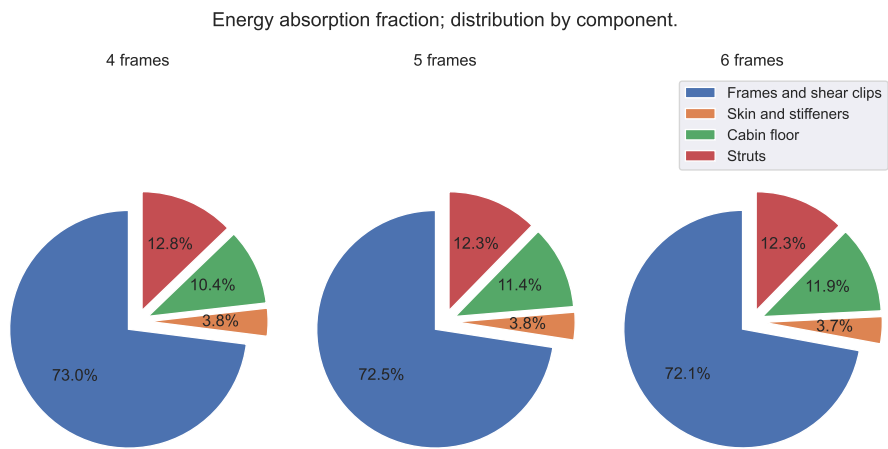
Fig. A.5: Energy fraction absorbed by each component, for a different number of frames sections.

B. Pre- and post-crash sections comparison

4S-1, best, undeformed. t_s = 2.0 mm, t_b = 1.0mm   4S-1, best, deformed
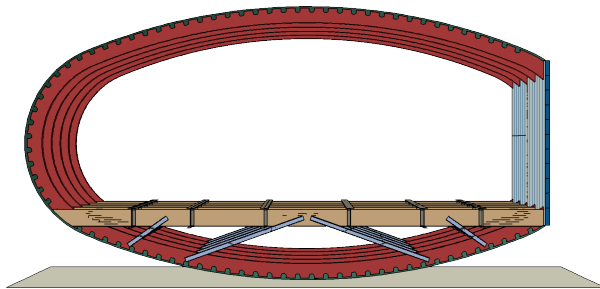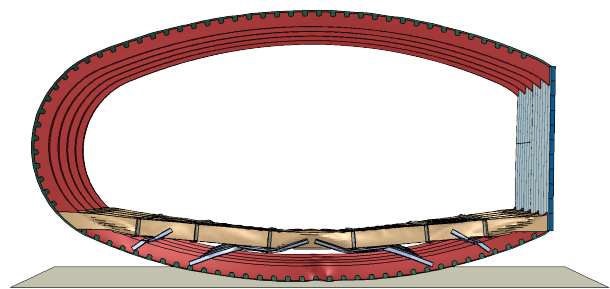
4S-2, best, undeformed. t_s = 2.0 mm, t_b = 1.0mm   4S-2, best, deformed
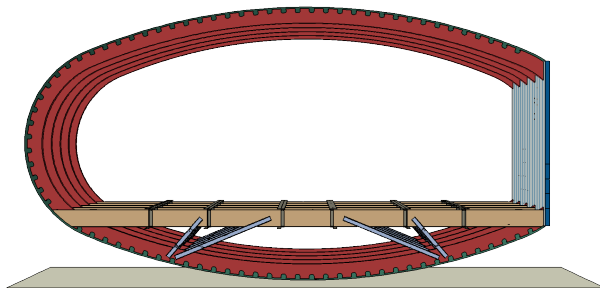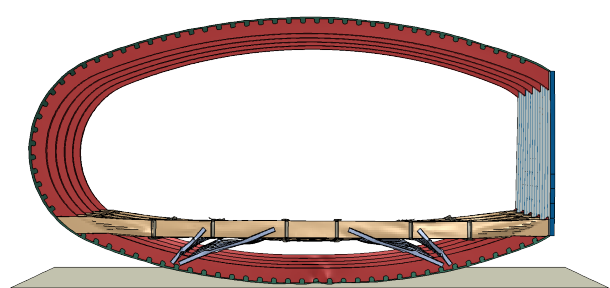
Fig. B.1: Undeformed and deformed FV crash sections, 4S concept (4S-1 and 4S-2), best configurations. Different colors are indicative of different section assignments. t_s and t_b indicate the shell thickness of the floor struts and the floor beams, respectively. Fuselage frames, due to their high bending stiffness, do not deform significantly, and, thus, the impact is dissipated thru the buckling of the floor beam and floor struts.

4S-3, best, undeformed. t_s = 2.5 mm, t_b = 1.0mm   **4S-3, best, deformed**
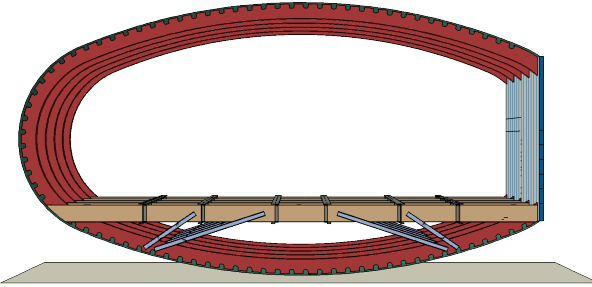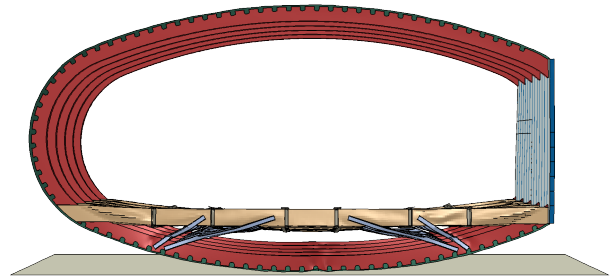
4S-4, best, undeformed. t_s = 2.5 mm, t_b = 1.0mm   **4S-4, best, deformed**
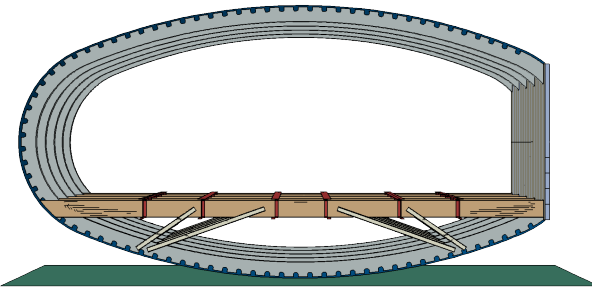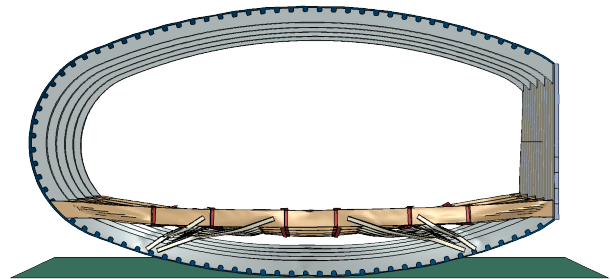
4S-5, best, undeformed. t_s = 2.0 mm, t_b = 1.0mm   **4S-5, best, deformed**
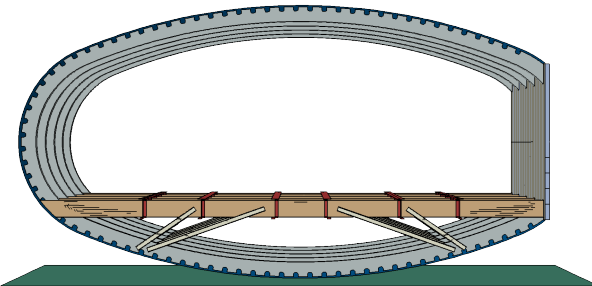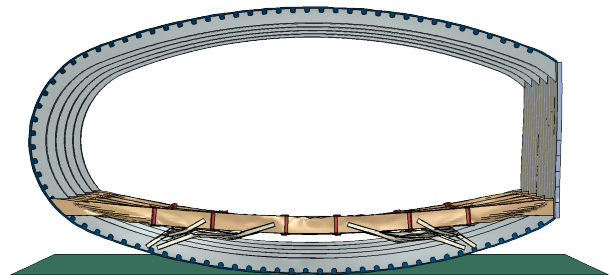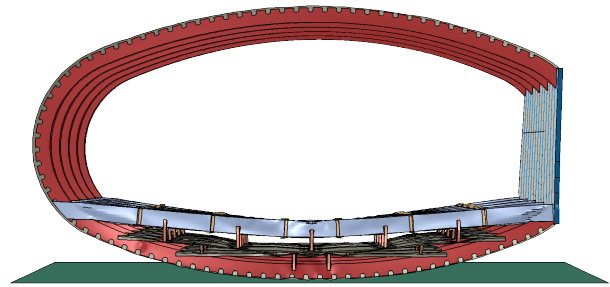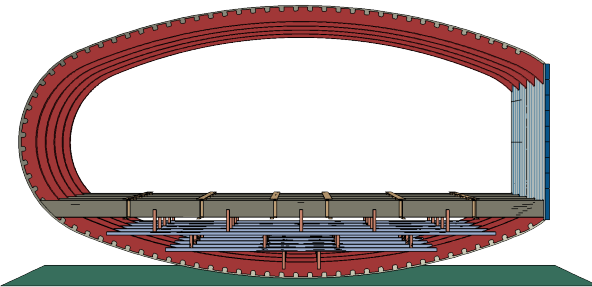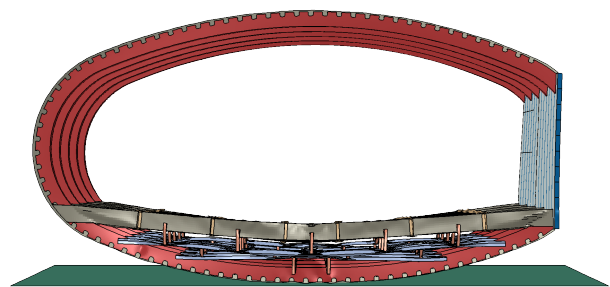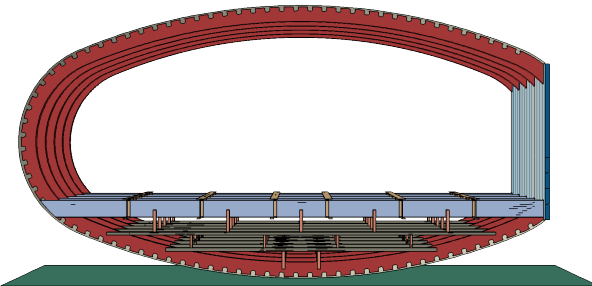

Fig. B.2: Undeformed and deformed FV crash sections, 4S concept (4S-3 to 4S-5), best configurations. Different colors are indicative of different section assignments. t_s and t_b indicate the shell thickness of the floor struts and the floor beams, respectively. Fuselage frames, due to their high bending stiffness, do not deform significantly, and, thus, the impact is dissipated thru the buckling of the floor beam and floor struts.

HB-1, best, undeformed. t_s = 2.5 mm, t_b = 1.0mm, t_v = 1.5mm, t_h = 2mm　　　HB-1, best, deformed
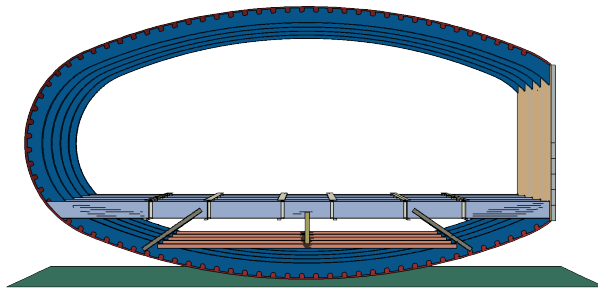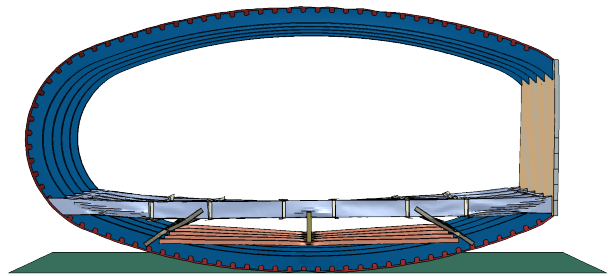
HB-2, best, undeformed. t_s = 1.5 mm, t_b = 1.5mm, t_v = 0.75mm, t_h = 1.0mm　　　HB-2, best, deformed
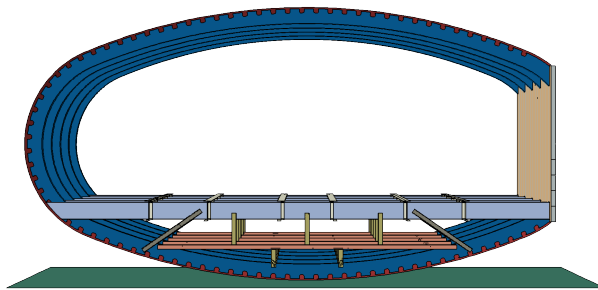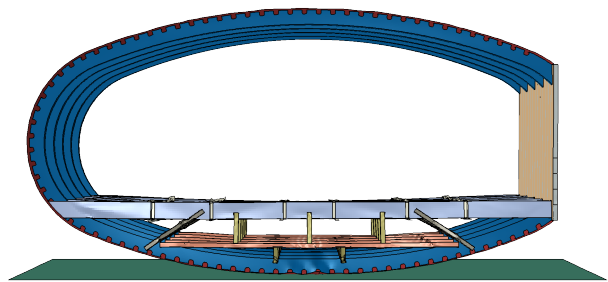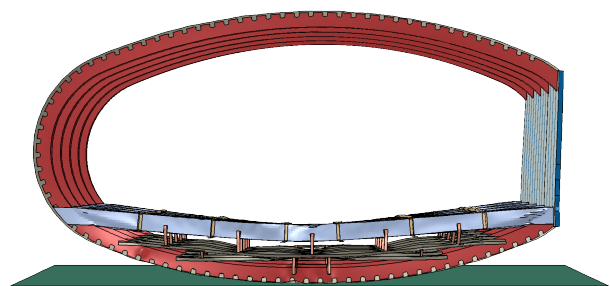
Fig. B.3: Undeformed and deformed FV crash sections, HB concept (HB-1 and HB-2), best configurations. Different colors are indicative of different section assignments. t_s and t_b indicate the shell thickness of the (oblique) floor struts and the floor beams, while t_v and t_h those of the vertical struts and horizontal beam, respectively. HB-1: limited plastic deformation of both the horizontal beam and the vertical strut. HB-2: good crushing of the vertical struts below the horizontal beam, but poor plastic deformation of those above.

HB-3, best, undeformed. t_s = 2.5 mm, t_b = 1.0mm, t_v = 0.5mm, t_h = 1.5mm   HB-3, best, deformed
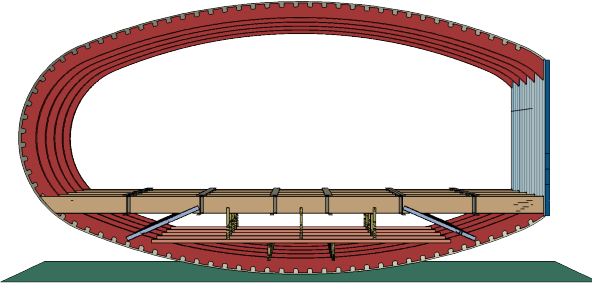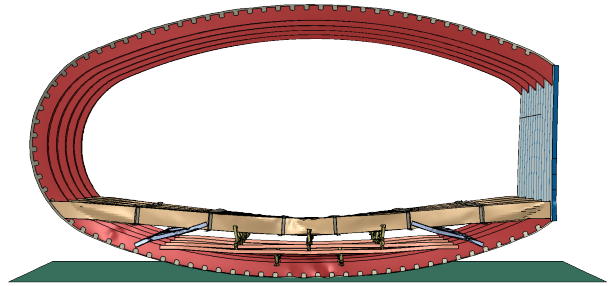
HB-4, best, undeformed. t_s = 1.5 mm, t_b = 1.5mm, t_v = 0.5mm, t_h = 0.5mm   HB-4, best, deformed
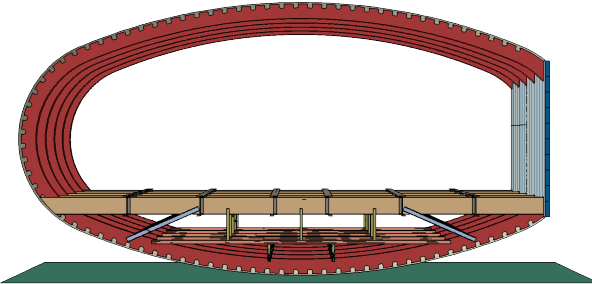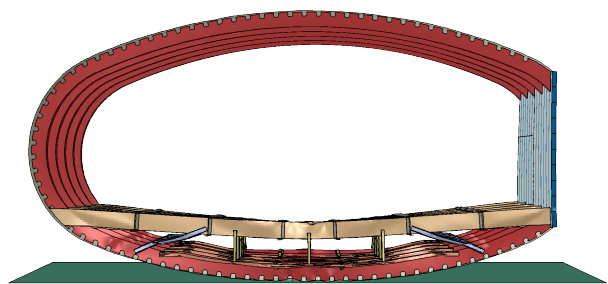
HB-5, best, undeformed. t_v = 0.75mm, t_h = 0.75mm   HB-5, best, deformed
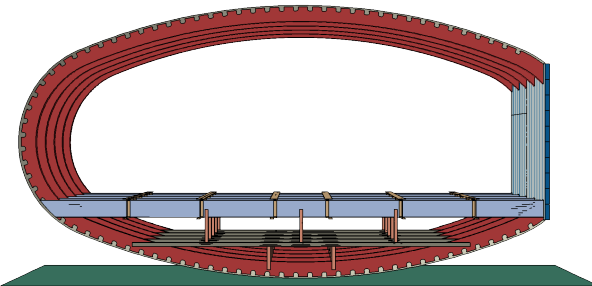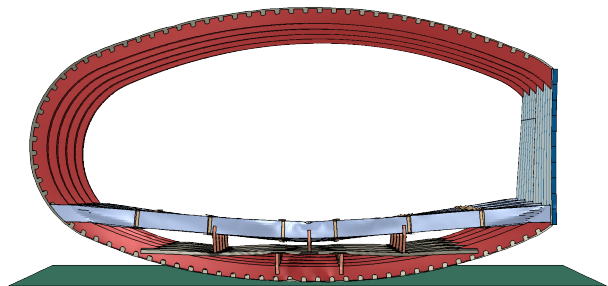
Fig. B.4: Undeformed and deformed FV crash sections, HB concept (HB-3 to HB-5), best configurations. Different colors are indicative of different section assignments. t_s and t_b indicate the shell thickness of the (oblique) floor struts and the floor beams, while t_v and t_h those of the vertical struts and horizontal beam, respectively. HB-3: all elements are plastically deforming and thus contributing to dissipate energy. HB-4: the cross-section of the horizontal beam has been reduced and, thus, it collapses due to bending instability. HB-5: crash concept without oblique struts. Energy is absorbed thru Euler buckling of the vertical struts.

HBH-1, best, undeformed. t_v = 0.5mm, t_h = 0.5mm   HBH-1, best, deformed
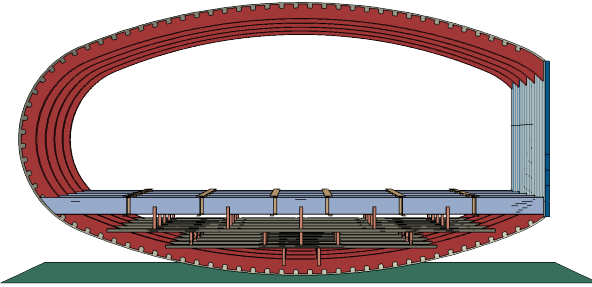
HBH-2, best, undeformed. t_v = 0.5mm, t_h = 0.5mm   HBH-2, best, deformed

HBH-3, best, undeformed. t_v = 0.5mm, t_h = 0.5mm   HBH-3, best, deformed

Fig. B.5: Undeformed and deformed FV crash sections, HBH concept (HBH-1 to HBH-3), best configurations. Different colors are indicative of different section assignments. t_v and t_h indicate the shell thickness of the vertical struts and horizontal beams, respectively. All configurations perform poorly as their are affected by structural instability (torsion about the horizontal beams).
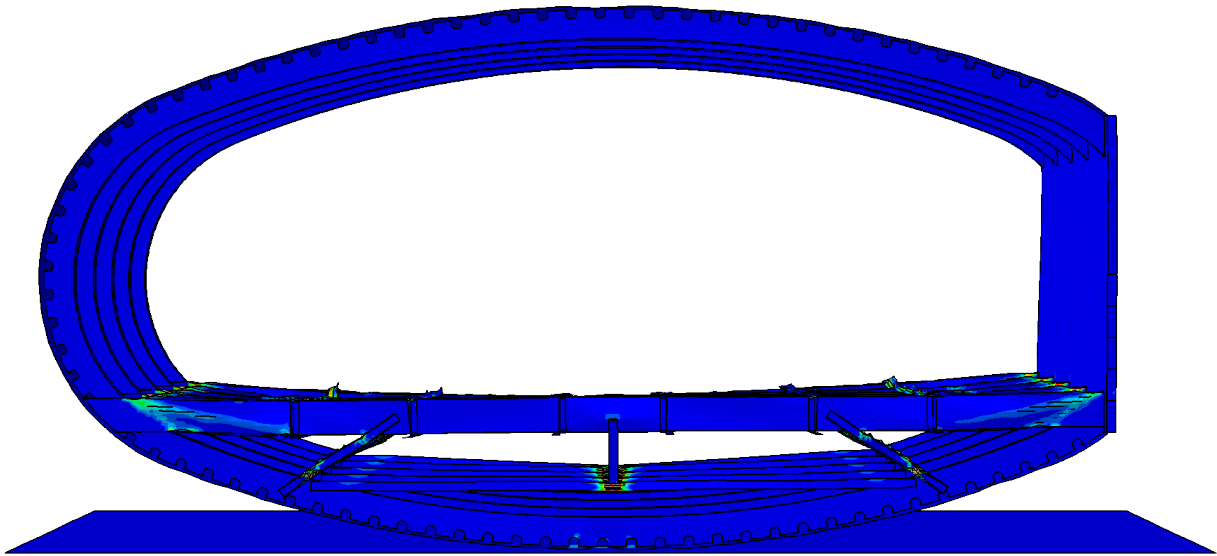
Fig. B.6: Equivalent plastic strain, HB-1, t_v =1.5 mm, t_h =1.5 mm
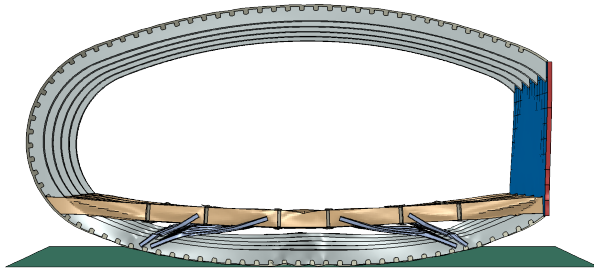
Fig. B.7: Mesh sensitivity analysis, 0.80x, post-crash.
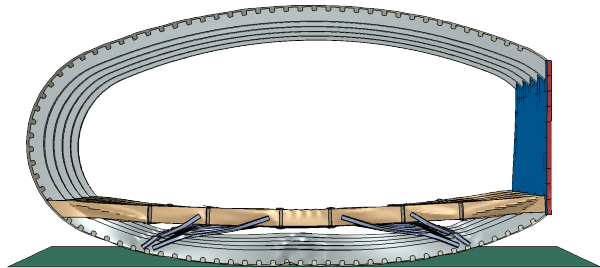
Fig. B.8: Mesh sensitivity analysis, 0.90x, post-crash.
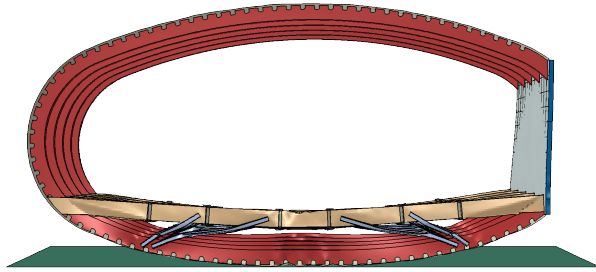
Fig. B.9: Sensitivity analysis: FB thickness 1.25mm, post-crash.
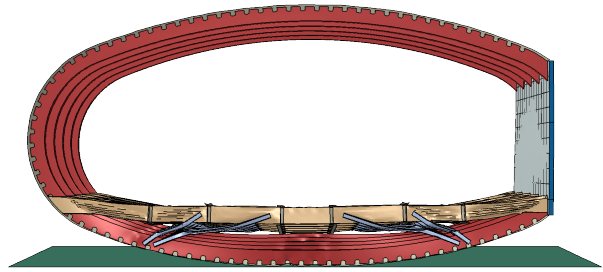
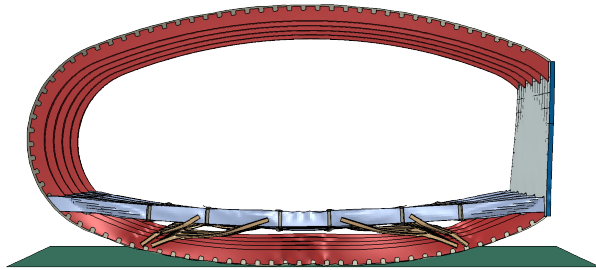**Fig. B.10:** Sensitivity analysis: FB thickness 0.75mm, post-crash.

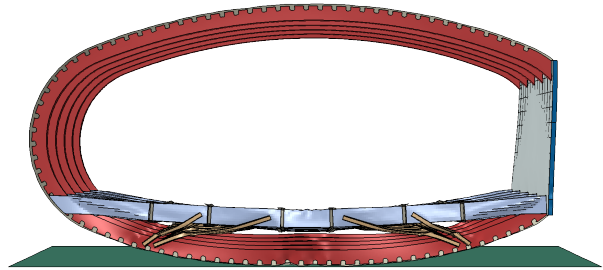**Fig. B.11:** Sensitivity analysis: Floor Beam Flange Width-to-Web Height Ratio of 2, post-crash.

Fig. B.12: Sensitivity analysis: Floor Beam Flange Width-to-Web Height Ratio of 4, post-crash.
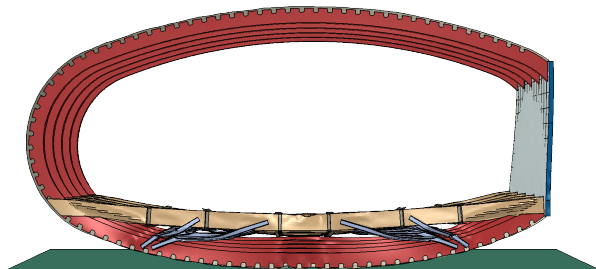

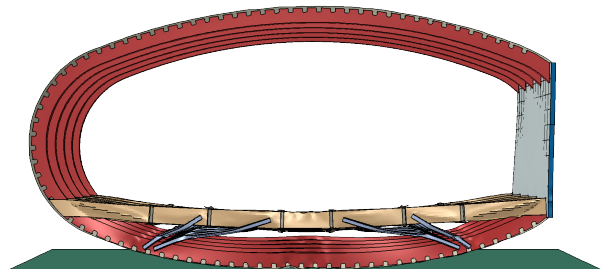**Fig. B.13:** Sensitivity analysis: FS thickness 2.25mm, post-crash.

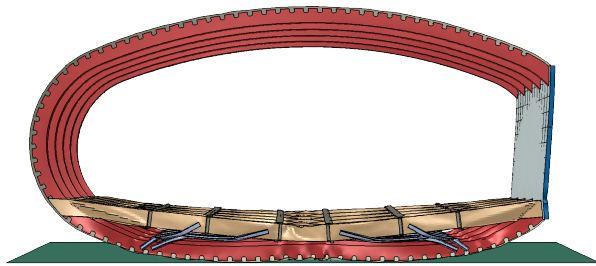**Fig. B.14:** Sensitivity analysis: FS thickness 2.75mm, post-crash.

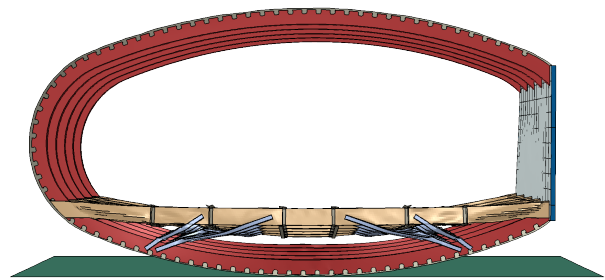**Fig. B.15:** Sensitivity analysis: frames thickness 4.7mm, post-crash.

Fig. B.16: Sensitivity analysis: frames thickness 6.7mm, post-crash.